การย่อยสลายไดยูรอนแบบโฟโตอิเล็กโตรแคตาไลติกบนฟิล์มไทเทเนีย

นายธีรภัทร รักษาธรรม

จุฬาลงกรณ์มหาวิทยาลัย
Chulalongkorn University

วิทยานิพนธ์นี้เป็นส่วนหนึ่งของการศึกษาตามหลักสูตรปริญญาวิศวกรรมศาสตรมหาบัณฑิต
สาขาวิชาวิศวกรรมเคมี ภาควิชาวิศวกรรมเคมี
คณะวิศวกรรมศาสตร์ จุฬาลงกรณ์มหาวิทยาลัย
ปีการศึกษา 2556
ลิขสิทธิ์ของจุฬาลงกรณ์มหาวิทยาลัย

บทคัดย่อและแฟ้มข้อมูลฉบับเต็มของวิทยานิพนธ์ตั้งแต่ปีการศึกษา 2554 ที่ให้บริการในคลังปัญญาจุฬาฯ (CUIR)
เป็นแฟ้มข้อมูลของนิสิตเจ้าของวิทยานิพนธ์ ที่ส่งผ่านทางบัณฑิตวิทยาลัย
The abstract and full text of theses from the academic year 2011 in Chulalongkorn University Intellectual Repository (CUIR)
are the thesis authors' files submitted through the University Graduate School.

PHOTOELECTROCATALYTIC DEGRADATION OF DIURON ON TITANIA FILM

Mr. Teerapat Raksatham

จุฬาลงกรณ์มหาวิทยาลัย
Chulalongkorn University

A Thesis Submitted in Partial Fulfillment of the Requirements
for the Degree of Master of Engineering Program in Chemical Engineering
Department of Chemical Engineering
Faculty of Engineering
Chulalongkorn University
Academic Year 2013

Copyright of Chulalongkorn University

Thesis Title	PHOTOELECTROCATALYTIC DEGRADATION OF DIURON ON TITANIA FILM
By	Mr. Teerapat Raksatham
Field of Study	Chemical Engineering
Thesis Advisor	Assistant Professor Varong Pavarajarn, Ph.D.

Accepted by the Faculty of Engineering, Chulalongkorn University in Partial Fulfillment of the Requirements for the Master's Degree

.....Dean of the Faculty of Engineering

(Professor Bundhit Eua-arporn, Ph.D.)

THESIS COMMITTEE

.....Chairman

(Associate Professor Prasert Pavasant, Ph.D.)

.....Thesis Advisor

(Assistant Professor Varong Pavarajarn, Ph.D.)

.....Examiner

(Assistant Professor Apinan Soottitantawat, D.Eng.)

.....External Examiner

(Chanchana Thanachayanont, Ph.D.)

จุฬาลงกรณ์มหาวิทยาลัย
Chulalongkorn University

ธีรภัทร รักษาธรรม : การย่อยสลายไดยูรอนแบบโฟโตอิเล็กโตรแคตาไลติกบนฟิล์มไทเทเนีย. (PHOTOELECTROCATALYTIC DEGRADATION OF DIURON ON TITANIA FILM) อ.ที่ปรึกษาวิทยานิพนธ์หลัก: ผศ. ดร.วรงค์ ปวราจารย์, 85 หน้า.

ไดยูรอนถูกใช้เป็นสารกำจัดวัชพืชที่ใช้กันอย่างแพร่หลายในประเทศไทย ไดยูรอนมีความเป็นพิษและยากต่อการย่อยสลาย ทำให้เกิดการปนเปื้อนในดินและแหล่งน้ำ ในงานวิจัยนี้ไดยูรอนถูกกำจัดด้วยปฏิกิริยาโฟโตอิเลคโตรแคตาไลติกซึ่งเป็นการทำงานร่วมกันระหว่างปฏิกิริยาโฟโตแคตาไลติกและอิแลคโตไลติก โดยใช้ไทเทเนียที่สังเคราะห์ด้วยวิธีโซลเจลแล้วเคลือบบนแผ่นไทเทเนียมเป็นขั้วแอโนดและใช้แผ่นแกรไฟต์เป็นขั้วแคโทด โดยได้ใช้การทดลองออกแบบชนิดบ็อกซ์ – แบงเก็น ในการวิเคราะห์ผลกระทบของค่าความต่างศักย์ ค่าความเป็นกรด - ด่าง และคลอไรด์ไอออนที่มีต่อการย่อยสลายไดยูรอน พบว่าประสิทธิภาพความสัมพันธ์ระหว่างค่าความเป็นกรด – ด่างกับค่าความต่างศักย์และคลอไรด์ไอออน ส่งผลกระทบต่อประสิทธิภาพการย่อยสลายไดยูรอน ในขณะที่ค่าคงที่ของอัตราการเกิดปฏิกิริยาจะขึ้นอยู่กับค่าความเป็นกรด – ด่างและคลอไรด์ไอออน

จุฬาลงกรณ์มหาวิทยาลัย
Chulalongkorn University

ภาควิชา วิศวกรรมเคมี ลายมือชื่อนิสิต .....

สาขาวิชา วิศวกรรมเคมี ลายมือชื่อ อ.ที่ปรึกษาวิทยานิพนธ์หลัก .....

ปีการศึกษา 2556

5570241221 : MAJOR CHEMICAL ENGINEERING
KEYWORDS: DIURON / PHOTOELECTROCATALYTIC / DEGRADATION / TITANIA FILM / RSM - BBD

TEERAPAT RAKSATHAM: PHOTOELECTROCATALYTIC DEGRADATION OF DIURON ON TITANIA FILM. ADVISOR: ASST. PROF. VARONG PAVARAJARN, Ph.D., 85 pp.

Diuron is an herbicide generally used in Thailand. It is persistent and highly toxic. Thus, diuron has leaded to contamination problems in soil and water. In this study, photoelectrocatalysis (PEC), which is a coupling between photocatalysis and electrolysis, was used to degrade diuron in water, using titania as a photocatalyst. Titania was synthesized via sol-gel method and was coated on a titanium substrate that was used as the anode. On the other side of the system, a graphite plate was placed as the cathode. Box – Behnken design (BBD) was used to describe effect of applied voltage, pH, and chloride ion on the diuron degradation. As the results, efficiency of diuron degradation depends on pH, chloride ion and applied voltage, while apparent rate constant depends on pH and chloride ion.

จุฬาลงกรณ์มหาวิทยาลัย
Chulalongkorn University

Department: Chemical Engineering Student's Signature .....
Field of Study: Chemical Engineering Advisor's Signature .....
Academic Year: 2013

ACKNOWLEDGEMENTS

I would like to express my sincere gratitude to my advisor, Asst. Prof. Dr.Varong Pavarajarn. For his, invaluable suggestion and encouragement to pass by the problems and obstacles.

I would like to thank Dr.Chanchana Thanachayanont for provide advice and suggestion to my research.

I would grateful to thank to Assc. Prof. Dr.Prasert Pavasant as the chairman, Asst. Prof. Dr.Apinan Sootitantawat as the thesis committee for their cooperation, comment, and discussions.

I thank Ms. Chabaiporn Junin for teaching me how to synthesized titania film, guidance and assistance throughout the duration of my research.

I thank all my members of the Center of Excellent in Particle Technology and friends who provide the support and encouragement always my research

Finally, I especially want to devote this thesis to my parents. They have pushed toward to unconditionally give me help and encouragement in order to gain this accomplishment.

จุฬาลงกรณ์มหาวิทยาลัย
Chulalongkorn University

CONTENTS

Page

THAI ABSTRACT iv
ENGLISH ABSTRACT v
ACKNOWLEDGEMENTS vi
CONTENTS vii
CONTENT OF TABLES ix
CONTENT OF FIGURES x
CHAPTER I INTRODUCTION 1
CHAPTER II THEORY AND LITERATURE REVIEWS 4
2.1 Diuron 4
2.2 Titania (TiO_2) 5
2.3 Photoeletrocatalysis 7
2.4 Box – Behngen Design (BBD) 10
CHAPTER III EXPERIMENTAL 12
3.1 Materials 12
3.2 Apparatus 12
3.3.1 Preparation of titanium substrate 13
3.3.2 Fabrication of titania film 13
3.4 Characterizations 14
3.5 Degradation of diuron 15
CHAPTER IV RESULTS AND DISCUSSION 16
4.1 Characteristics of titania film 16
4.2 2^k – factorial design 19
4.3 Effect of applied voltage of diuron degradation 27
4.4 Effect of pH and applied voltage of diuron degradation 34
4.5 Effect of applied voltage, pH, and chloride ion on diuron degradation 45
CHAPTER V CONCLUSION 61
5.1 Summary of the results 61

จุฬาลงกรณ์มหาวิทยาลัย
CHULALONGKORN UNIVERSITY

Page

5.2 Conclusions 61
5.3 Recommendations for future work 61
REFERENCES 62
APPENDICES 65
APPENDIX A CALIBRATION CURVE OF DIURON 66
APPENDIX B CALIBRATION CURVE OF NITRATE 67
APPENDIX C CALIBRATION CURVE OF NITRITE 68
APPENDIX D CALCULATION OF THE CRYSTALLITE SIZE 69
APPENDIX E CALCULATION OF PHASE COMPOSITION OF TITANIA 71
APPENDIX F CODING DATA 73
APPENDIX G CALCULATION OF MAIN AND INTERACTION EFFECT 74
APPENDIX H NORMAL PROBABILITY PLOT 76
APPENDIX I PRECISION OF CALCULATED EFFECT 78
APPENDIX J ANOVA TABLE 80
APPENDIX K TOTAL ORGANIC COMPOUND 82
APPENDIX L LIST OF PLUBLICATION 84
VITA 85

จุฬาลงกรณ์มหาวิทยาลัย
Chulalongkorn University

CONTENT OF TABLES

Page

Table 2.1 Chemical identity and physical properties of diuron. 5
Table 2.2 Physical and structural properties of anatase and rutile. 7
Table 4.1 Crystalline size and phase composition percentage. 18
Table 4.2 Factors and levels in 3 factors 2^k - factorial design. 19
Table 4.3 The condition and response of test run. 19
Table 4.4 Factor values. 20
Table 4.5 The apparent rate constants of photoelectrocatalysis at pH 7. 31
Table 4.6 The apparent rate constants of electrolysis at pH 7. 31
Table 4.7 The apparent rate constants of photoelectrocatalysis under applied voltage of 5 V. 36
Table 4.8 The apparent rate constants of photoelectrocatalysis at pH 3. 38
Table 4.9 The apparent rate constants of electrolysis at pH 3. 38
Table 4.10 The apparent rate constants of photoelectrocatalysis at pH 11. 39
Table 4.11 The apparent rate constants of electrolysis at pH 11. 40
Table 4.12 Factors and levels in the three – factors three – levels BBD design 46
Table 4.13 Design of BBD and responses. 47
Table 4.14 ANOVA for the RSM model for diuron degradation percentage. 48
Table 4.15 ANOVA for the RSM model for k_{app} at 120 minute. 55
Table G1 The level of the factor. 74
Table H1 Cumulative probability. 76
Table I1 Confidence interval of calculated effect. 79
Table J1 The equation of ANOVA. 80

จุฬาลงกรณ์มหาวิทยาลัย
Chulalongkorn University

CONTENT OF FIGURES

Page

Figure 2.1 Structure of diuron. 4
Figure 2.2 Crystal structures of TiO_2 (a) Rutile, (b) Anatase, and (c) Brookite. 6
Figure 2.3 Schematic of photoelectrocatalysis on anode. 8
Figure 2.4 Schematic of photoelectrocatalysis on cathode. 8
Figure 2.5 Three factor Box – Behnken design (coded factor levels). 11
Figure 3.1 Schematic diagram of the degradation system. 13
Figure 4.1 SEM images (a) before being calcined 500°C and 16
Figure 4.2 XRD patterns of titania film (a) before calcined 500°C and 18
Figure 4.3 Calculated effect bar plot 21
Figure 4.4 Normal probability plots 22
Figure 4.5 Precision of calculated effect 23
Figure 4.6 Efficiency of the diuron degradation with and without nitrate ion 24
Figure 4.7 Efficiency of the diuron degradation with and without nitrate ion 24
Figure 4.8 Nitrate concentration under pH 7 and applied voltage 0.5 V. 26
Figure 4.9 Nitrite concentration under pH 7 and applied voltage 0.5 V. 26
Figure 4.10 Effect of applied voltage for diuron degradation. 29
Figure 4.11 First – order linear transforms plot of the photoelectrocatalytic degradation at pH 7. 30
Figure 4.12 HPLC peak height of intermediates generated during photoelectrocatalytic degradation of diuron at applied voltage 2.5 V. 32
Figure 4.13 HPLC peak height of intermediates generated during photoelectrocatalytic degradation of diuron at applied voltage 5 V. 33
Figure 4.14 HPLC peak height of intermediates generated during photoelectrocatalytic degradation of diuron at applied voltage 7.5 V. 33
Figure 4.15 HPLC peak height of intermediates generated during photoelectrocatalytic degradation of diuron at applied voltage 10 V. 34
Figure 4.16 Effect of pH for diuron degradation under applied voltage 5 V. 35
Figure 4.17 Effect of pH for diuron degradation under various applied voltage. 37

Page

Figure 4.18 First – order linear transforms plot of the photoelectrocatalytic degradation at pH 3. 37
Figure 4.19 First – order linear transforms plot of the photoelectrocatalytic degradation at pH 11. 39
Figure 4.20 HPLC peak heights of intermediates generated during photoelectrocatalytic degradation of diuron under pH 3 and applied voltage 2.5 V. 41
Figure 4.21 HPLC peak heights of intermediates generated during photoelectrocatalytic degradation of diuron under pH 3 and applied voltage 5 V. ... 41
Figure 4.22 HPLC peak heights of intermediates generated during photoelectrocatalytic degradation of diuron under pH 3 and applied voltage 7.5 V. 42
Figure 4.23 HPLC peak heights of intermediates generated during photoelectrocatalytic degradation of diuron under pH 3 and applied voltage 10 V. . 42
Figure 4.24 HPLC peak heights of intermediates generated during photoelectrocatalytic degradation of diuron under pH 11 and applied voltage 2.5 V. 43
Figure 4.25 HPLC peak heights of intermediates generated during photoelectrocatalytic degradation of diuron under pH 11 and applied voltage 5 V. . 43
Figure 4.26 HPLC peak heights of intermediates generated during photoelectrocatalytic degradation of diuron under pH 11 and applied voltage 7.5 V. 44
Figure 4.27 HPLC peak heights of intermediates generated during photoelectrocatalytic degradation of diuron under pH 11 and applied voltage 10 V. 44
Figure 4.28 Residual plot of diuron degradation percentage. 49
Figure 4.29 Comparison diuron degradation percentages between the predicted values and the actual values of RSM – BBD model. 49
Figure 4.30 Chloride ion concentration and pH 3D surface and Chloride ion concentration and pH contour of predicted degradation percentage. 50
Figure 4.31 Chloride ion concentration and applied voltage 3D surface and Chloride ion concentration and applied voltage contour of predicted degradation percentage. 50

Page

Figure 4.32 pH and applied voltage 3D surface and pH and applied voltage contour of predicted degradation percentage. 51
Figure 4.33 Predicted degradation percentages via the mathematical model under applied voltage 2.5 V. 52
Figure 4.34 Predicted degradation percentages via the mathematical model under concentration of chloride ion 625 ppm. 53
Figure 4.35 Predicted degradation percentages via the mathematical model under pH 7. 53
Figure 4.36 Residual plot of the apparent rate constant at 120 minute. 55
Figure 4.37 Comparison the apparent rate constant at 120 minute between the predicted values and the actual values of RSM – BBD model. 56
Figure 4.38 Chloride ion concentration and pH 3D surface and Chloride ion concentration and pH contour of predicted the apparent rate constant at 120 minute. 56
Figure 4.39 Chloride ion concentration and applied voltage 3D surface and Chloride ion concentration and applied voltage contour of predicted the apparent rate constant at 120 minute. 57
Figure 4.40 pH and applied voltage 3D surface and pH and applied voltage contour of predicted the apparent rate constant at 120 minute. 57
Figure 4.41 Predicted the apparent rate constant at 120 minute via the mathematical model under applied voltage 0.5 V. 58
Figure 4.42 Predicted the apparent rate constant at 120 minute via the mathematical model under concentration of chloride ion 625 ppm. 59
Figure 4.43 Predicted the apparent rate constant at 120 minute via the mathematical model under pH 7. 59
Figure A1 Calibration curve of diuron. 66
Figure B1 Calibration curve of nitrate. 67
Figure C1 Calibration curve of nitrite. 68
Figure D1 The observation peak of anatase phase for calculating the crystallite size. 69

Page

Figure E1 The observation peak of anatase phase for calculating phase composition. 72
Figure E2 The observation peak of rutile phase for calculating phase composition. .. 72
Figure H1 Cumulative probability plot. 77
Figure I1 Confidence interval of calculated effect plot. 79
Figure K1 TOC under applied voltage 2.5 V. 82
Figure K2 TOC under applied voltage 5 V. 82
Figure K3 TOC under applied voltage 7.5 V. 83
Figure K4 TOC under applied voltage 10 V. 83

จุฬาลงกรณ์มหาวิทยาลัย
Chulalongkorn University

CHAPTER I

INTRODUCTION

Diuron (3 - (3, 4 - dichlorophenyl) - 1, 1 - dimethylurea) is an herbicide in the phenylurea family which is widely used in agriculture. It restricts creation of oxygen and prevents transfer of electron in photosynthesis in herbage whereas some parts of it are contaminated in soil and water, resulting in soil and water pollution [1-3]. Diuron has high toxicity and is rarely decomposed in environment. Moreover, intermediates that are produced from diuron break – down sometimes are more poisonous [4, 5].

There are many techniques to remove diuron from water such as hydrolysis, biological microbe degradation, adsorption, and photocatalysis. The photocatalytic method is commonly used to degrade organic pollutant. Catalyst produces electrons and holes when it is encouraged by light. Both electrons and holes create oxidizing agents. Despite high efficiency and short time for diuron degradation, recombination between electrons and holes leads to a decreased rate of diuron removal.

จุฬาลงกรณ์มหาวิทยาลัย
CHULALONGKORN UNIVERSITY

Photoelectrocatalysis is a combination between photocatalytic and electrolytic reactions. When a photocatalyst is excited by photon with energy higher than the band gap, an electron is moved from the valance band to the conduction band leaving the position of electron shortage to become a hole. After that, electrons and holes are separated by electrolytic reaction so that recombination between photoexcited electrons and holes is decreased. Water is attacked on anode by holes. It becomes hydroxyl radicals and subsequently oxidizes pollutant in water.

Electrons are transferred to cathode and released to oxygen, to form superoxide radical.

Among the catalysts used in the photocatalytic processes, titania (TiO_2) is the most popular catalyst since it has photostability, ability to break structure of organic compounds, non – toxic, and low cost [6]. Nevertheless, titania in power form is hard to be removed treated water. To solve this problem, titania can be coated on substrate as thin film. However, surface area will be reduced which will affect the rate of degradation.

In this study, titania was immobilized on titanium sheet. It was used as an anode in photoeletrocatalytic reaction, in which graphite was used as a cathode. The application on diuron degradation was tested over this system under various conditions.

It is aims of this study, to study degradation of diuron via photoelectrocatalytic technique and to investigate the effect of parameters used in the diuron degradation.

This thesis has five chapters as following:

Chapter I proposes the motivation and introduction of this work.

Chapter II explains theory and literature reviews relating to chemical and physical properties of diuron and titania as well as mechanism of photoelectrocatalytic process.

Chapter III consists of chemicals, materials, and apparatus used in the experiment as well as, characterizations, and experimental procedure.

Chapter IV describes and discusses the experimental results.

จุฬาลงกรณ์มหาวิทยาลัย
Chulalongkorn University

Chapter V concludes the overall results of this work and guide for future research.

จุฬาลงกรณ์มหาวิทยาลัย
CHULALONGKORN UNIVERSITY

CHAPTER II

THEORY AND LITERATURE REVIEWS

Theory and literature reviews relating to chemical and physical properties of diuron and titania and mechanism of photoelectrocatalytic reaction will be elaborated in this chapter.

2.1 Diuron

Agricultures were major industry in the world. These activities are still heavily involving herbicides. As a result, land and water are accumulated from them. These become soil and aqua pollutions. Weed killers are widely used and belong to the phenylurea family which has been liberally used for eliminate flora [7].

Diuron was white crystalline at room temperature. It was common herbicide for some grasses and broadleaved weeds and sometimes used in blending with other herbicides such as hexazinone paraquat, imazapyr, thiadiazuron, and bromacil. Structural formula of diuron is presented in Figure 2.1 while chemical identity and physical properties of diuron are shown in Table 2.1.

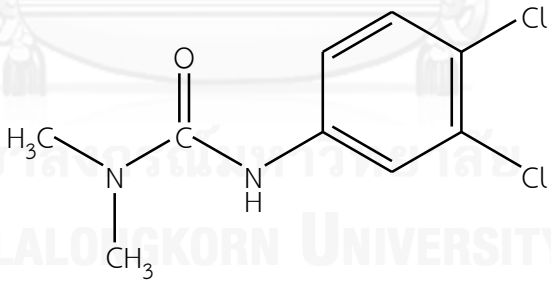

Figure 2.1 Structure of diuron.

Diuron is suddenly absorbed through the root system of plants and slowly diffuses through the stems and leaves. It is a strong inhibitor of the photosynthesis II system in plants via the Hill reaction (It involves the transfer of electrons from water to an electron acceptor that is created by the capture of light from chlorophyll A). The transfer of electrons from water to the electron acceptor is restrained hence the formations of NADPH (nicotinamide adenine dinucleotide phosphate) and ATP

(adenosine 5' – triphosphate) are obstructed. For many biochemical reactions in plants, both of NADPH and ATP are important [8].

Diuron is not absorbed by plants. It is residual in soil or washing leading to pollution problem. Diuron seldom decomposes in environment, nonetheless; there is a technique for removal diuron such as hydrolysis [4], biological degradation [9], and adsorption [10]. These methods have been used for a long time with low activities. Nowadays, advanced oxidation is popular because it has high efficiency and low cost [2, 11-13].

Table 2.1 Chemical identity and physical properties of diuron.

Common name	Diuron, DCMU
Chemical name – IUPAC	3-(3,4-dichlorophenyl)-1,1-dimethylurea
Chemical name – CAS	N'-(3,4-dichlorophenyl)-N,N-dimethylurea
CAS Registry Number	330-54-1
Molecular weight	233.09 g/mol
Molecular formula	$C_9H_{10}Cl_2N_2O$
Melting point	157 – 159°C
pKa	13.55
Solubility in water (25°C)	36.4 mg/l
Octanol water partition coefficient (pK_{ow}) (25°C)	2.85
Vapour pressure (25°C)	0.0011 mPa
Relative density	1.48
Henry's Law Constant	7.0×10^{-6} Pa·m^3/mol
Heat of vaporization	63.4 kJ/mol

จุฬาลงกรณ์มหาวิทยาลัย
CHULALONGKORN UNIVERSITY

2.2 Titania (TiO_2)

Titania (TiO_2), also known as titanium oxide, or titanium (IV) oxide is used for various applications. It is commonly used for photocatalyst because it has excellence stability against photocorrosion, nontoxicity, and low cost [14]. Moreover, it is used for filtrate pollutants and pathogen in air in industry. Titania has originally three phases, i.e. consisted of brookite, anatase, and rutile. Each phase has different structure and photoactivity. Anatase and rutile are widely used for photocatalyst but

anatase has the highest photocatalytic activities in theses morphology. Structure of titania is rearranged by chain of TiO_6. Ti^{4+} ion is enclosed by six oxygen ions (O^{2-}). All their morphology has contraction of arrangement in octahedra. All of structures are shown in Figure 2.2.

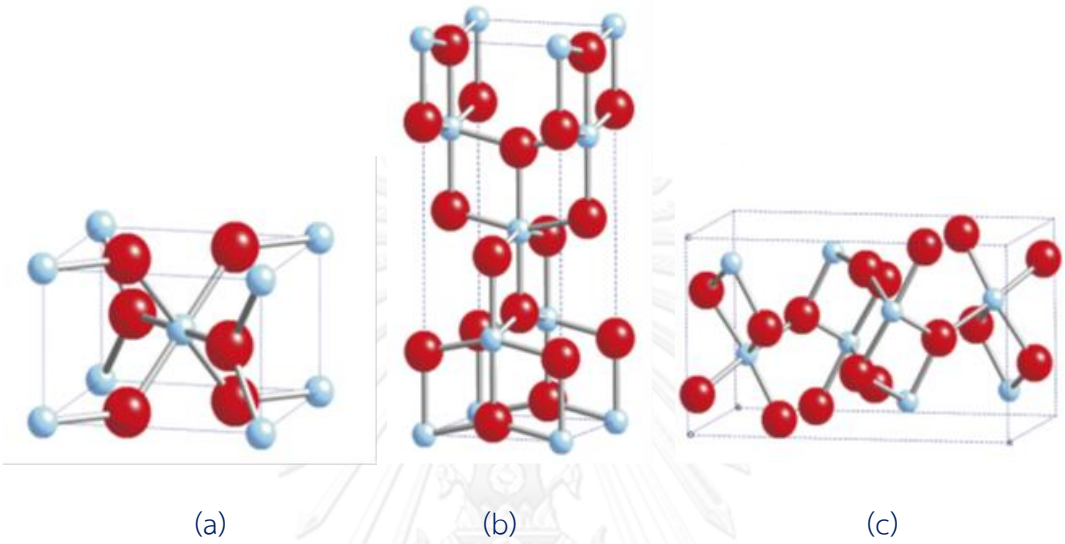

(a) (b) (c)

Figure 2.2 Crystal structures of TiO_2 (a) Rutile, (b) Anatase, and (c) Brookite.

Band gap energy of titania is 3.2, 3.0, and approximately 3.2 eV in anatase, rutile, and brookite phase, respectively. Before, titania is excited via photon. Electron and hole do not generate. When it is revived, electron jumps from conduction band to valence band. Free position on surface appears hole. Their properties are summarized in Table 2.2.

จุฬาลงกรณ์มหาวิทยาลัย
Chulalongkorn University

Table 2.2 Physical and structural properties of anatase and rutile.

Property	Anatase	Rutile
Boiling Point (°C)	N/A	2500 – 3000
Melting point (°C)	N/A	1825
Phase transformation temperature (°C)	600	N/A
Light absorption (nm)	< 390	< 415
Dielectric constant	31	114
Density (g/cm^3)	3.79	4.27
Refractive index	2.55	2.75
Crystalline structure	Quadratic	Quadratic
Mohr's Hardness	5.5	6.5 – 7.0
Ti – Ti distances (A°)	3.04 – 3.79	2.96 – 3.57
Ti – O distances (A°)	1.93 – 1.98	1.94 – 1.98
Absorption edge (nm)	385	405
Heat of formation	-933.0 (298K)	-944.7 (298K)
(ΔH^0_f), kJ/mol	-930.0 (1300K)	-942.4 (1300K)
Free energy of formation	-877.6 (298K)	-889.5 (298K)
(ΔG^0_f), kJ/mol	-697.4 (1300K)	-707.9 (298K)
Entropy (S), J/mol·K	49.9 (298K)	150.6 (298K)
	50.3 (1300K)	149.0 (1300K)

2.3 Photoeletrocatalysis

Photoelectrocatalytic reaction deceases effect of recombination between electron and hole via principle of electrical. Free electron moves under electric field when external energy is applied to electrode. This phenomenon induces electron; it separates to valence band on catalyst, so electron transfers from anode to cathode. As the result, electron releases excess energy in conduction band. It does not return to valence band. This method is extensively used for degradation organic pollutant in water because it has high efficiency and short time degradation [14]. Catalyst is usually semiconductor materials such as SnO_2, WO_3, ZnO, and TiO_2. They can be generate electron when encouraged by light.

Although, titania is widely used for research owing to high photoactivity, photostability, and low price. Efficiency drops when electron and hole merge. Applied voltage can be used to prevent it. Electron is induced under electric current. As a result, hole has still been appeared on surface. This phenomenon promotes degradation activity. These schematics are shown in Figure 2.3 – 2.4.

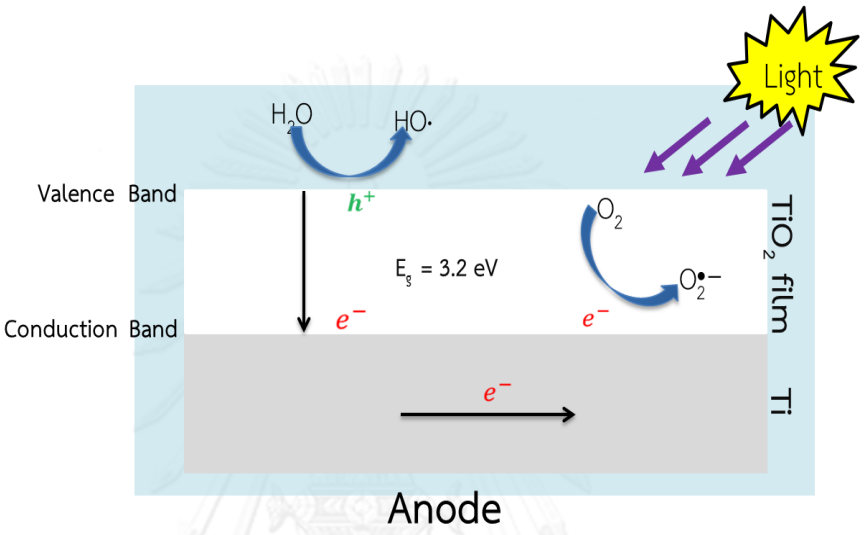

Figure 2.3 Schematic of photoelectrocatalysis on anode.

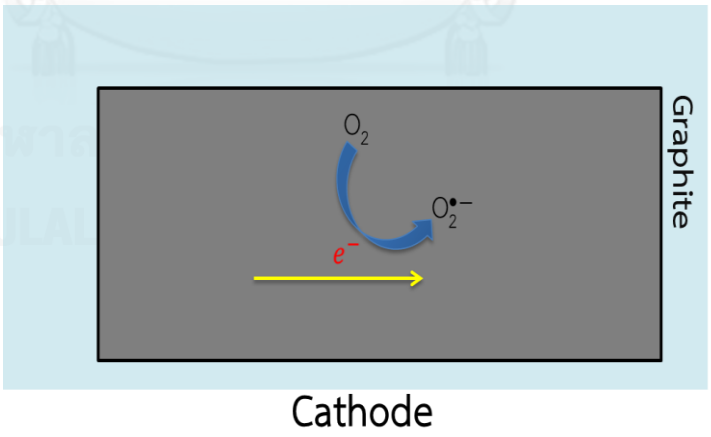

Figure 2.4 Schematic of photoelectrocatalysis on cathode.

Figure 2.3 – 2.4 present normal mechanisms on anode and cathode. In general, there are 8 different reactions occur on anode and cathode expressed as follows [15, 16].

i. Bandgap Energy (E_g) is instigated leading to formation of electron – hole charge pair on TiO_2.

$$TiO_2 + h\nu \longrightarrow e_{CB}^- + h^+ \qquad 2.3.1$$

ii. Electron moves to cathode while some electron recombines.

iii. Electron in conduction band is transferred to electron acceptor and dissolved oxygen.

$$e_{CB}^- + O_2 \longrightarrow O_2^-\cdot \qquad 2.3.2$$

iv. Hydroxyperoxyl radical is foremed from reductive pathway of oxygen.

$$O_2^-\cdot + H^+ \longrightarrow HO_2\cdot \qquad 2.3.3$$

v. Previous product attacks electron in conduction band and changes to hydrogenperoxide.

$$HO_2\cdot + H^+ + e_{CB}^- \longrightarrow H_2O_2 \qquad 2.3.4$$

vi. Hydroxyl radical creates from reaction between hydrogenperoxide and electron in conduction band.

$$H_2O_2 + e_{CB}^- \longrightarrow OH^- + OH\cdot \qquad 2.3.5$$

vii. Water adsorbed on the surface interacts with hole and generates hydroxyl radical.

$$h^+ + H_2O \longrightarrow OH\cdot + H^+ \qquad 2.3.6$$

viii. Intermediates are oxidized by hydroxyl radical.

In the past, photoelectrocatalytic was used for degradation of refractory organic pollants. For instance, Selcuk et al. determined potential bias for digestion of humic acid in which Ti/TiO_2 was used as electrode under UV light [17, 18]. Yan et al.

จุฬาลงกรณ์มหาวิทยาลัย
Chulalongkorn University

researched effect of pH and solution conductivity to decompose phenol in which TiO_2/Ni thin-film was used as electrode [19]. Their factors have impacted to degrade organic pollutant. Cardoso et al used to TNT's (titania nanotube) electrode for their study. Their work properly find a concentration of 4,4 - oxydianiline that it is removed under UV light [20].

2.4 Box – Behngen Design (BBD)

Experimental design is a powerful technique to predict the parameters that want to process because it gains increase knowledge of the existing process and optimizes these process. There are various methods in experimental design.

Box – Behngen dedign (BBD) is developed to reduce the weak points of Central Composite design (CCD) and Face – Central Composite design (FCCD). It is almost uniform design and still keeps factor values in interested range. The characteristic of this design is suitable for more three factors. The amount of experimental depends on the number of factor and center point run. It can be found from the follow equation:

$$\text{Number of test runs} = 2^k + 2^{k-1} + m$$

where k is number of factor ($k \geq 3$) and m is number of centre – point run.

The three factors Box – Behnken design is represented in Figure 2.5 and the full experimental model is used to explain by follow model.

$$\hat{y} = \beta_0 + \beta_1 A + \beta_2 B + \beta_3 C + \beta_{12} AB + \beta_{13} AC + \beta_{23} BC + \beta_{11} A^2 + \beta_{22} B^2 + \beta_{33} C^2$$

where $\hat{y}$ is response and β_i, β_{ij}, and β_{ii} are parameter of explanatory variables. A, B, and C was coded independent variables.

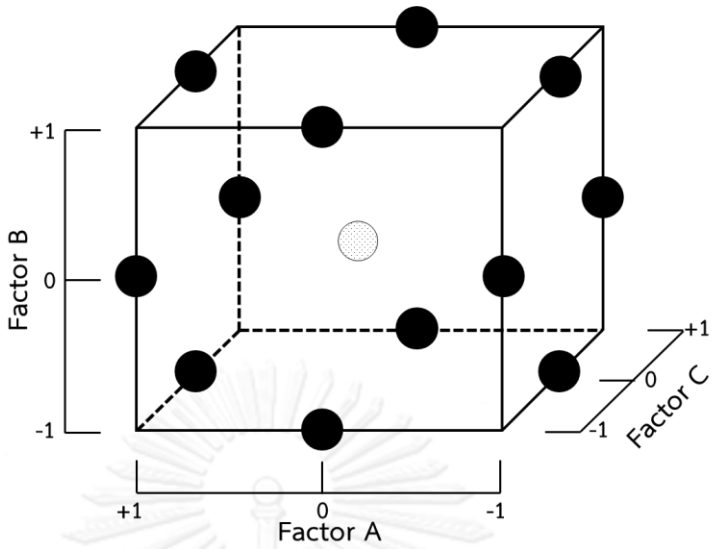

Figure 2.5 Three factor Box – Behnken design (coded factor levels).

However this method has disadvantage. When one parameter is eliminated, the model will be re – estimated due to co – variance of two parameters.

จุฬาลงกรณ์มหาวิทยาลัย
Chulalongkorn University

CHAPTER III
EXPERIMENTAL

This chapter gives detail of process in degradation of diuron. There are five main parts of experimental procedure that includes apparatus, materials, synthesis of TiO_2 film on titanium substrate, characterizations and degradation of diuron.

3.1 Materials

The chemicals used for synthesis TiO_2 film was titanium (IV) isopropoxide (97%, Sigma-Aldrich, Germany), isopropanol (99.9%, RCI Labscan, Thailand), acetylacetone (98%, Sigma-Aldrich, Germany), nitric acid (65%,), ethylcellulose (95%, Carlo erba reagents Co., France), and titania powder (P25, 99.9%, Sigma-Aldrich, Germany). The washing reagent used for cleaning titanium plate was acetone (99.5%, QReC, New Zealand) and methanol (99.9%, QReC, New Zealand). The diuron stock solution was prepared from diuron (99.5%, Sigma-Aldrich, Germany) dissolved in deionized water whereas hydrochloric acid (37%, QReC, New Zealand), sulfuric acid (98%, QReC, New Zealand), and sodium hydroxide (98%, Loba Chenie, India) were used for pH adjustment. Sodium chloride (99.9%, Ajax Finechem, Australia) was used to adjust conductivity of the solution. Furthermore, acetonitrile (99.9%, RCI Labscan, Thailand) was used as mobile phase in the analysis of diuron via high performance liquid chromatography (HPLC).

จุฬาลงกรณ์มหาวิทยาลัย
Chulalongkorn University

3.2 Apparatus

The schematic diagram of the equipment set up is shown in Figure 3.1. The system is consisting of 6 parts. First, a DC power supply was used to bias voltage for photoelectrocatalytic and electrolytic reactions. Second, 2 UV-A lamps (Phillips TLD 15W/05) were used as a light source of the photocatalysis and photoelectrocatalysis. Third, a magnetic stirrer was used to stir the solution. Next, 2 graphite sheets (5 cm X 10 cm in size) were used as cathode while 2 TiO_2/Ti plates (5 cm X 10 cm in size)

were used as anode. A 12 cm x 8 cm x 6 cm glass container was used as a reactor vessel. The reactor was placed in a box equipped with 2 fans used to control the ambient temperature.

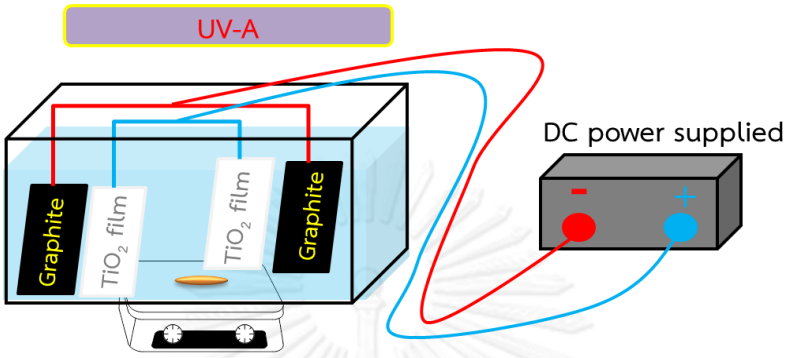

Figure 3.1 Schematic diagram of the degradation system.

3.3 Synthesis of TiO_2 film on titanium substrate

3.3.1 Preparation of titanium substrate

There were 5 steps to clean titanium plate, beginning with washing by detergent and being sonicated in acetone for 15 minutes. Later, the plate was sonicated in ethanol for 15 minutes. Next, it was sonicated in water for 3 times, each of which took 15 minutes. Finally, the substrate was blown with nitrogen gas.

จุฬาลงกรณ์มหาวิทยาลัย
Chulalongkorn University

3.3.2 Fabrication of titania film

Titania film was synthesized via sol – gel method and was screen-printed onto the substrate. The titanium (IV) isopropoxide (TTIP) of 4.5 ml was mixed in 15 ml isopropanol (IPA) and stirred continuously for 10 minutes. Then, 15 ml of acetylacetone (Acac) solution that was consisting of 0.925 ml Acac in IPA was added to the solution and stirred continuously for 10 minutes. Next, 10.92 µl of 65% nitric acid in 15 ml IPA was added to the solution and continuously stirred for 10 minutes. Later, 1 ml of 65% nitric acid was added to the solution and continuously stirred for 3 hours. After that, 3.37 ml of water, 1.95 g of ethylcellulose, and 6.73 g of P25 were

added to the solution. This mixture was rested overnight. Finally, it was coated on the titanium sheet by screen-printing and calcined at 500°C for 1 hour.

3.4 Characterizations

The crystalline structure and phase composition of tiania film were identified using X-ray Diffraction (XRD) (Bruker AXS D8 Advance) which was operated using CuKα radiation. The scan range was 2θ of 20 – 80° with a step size of 0.04° and a step time of 2.0 seconds. Voltage and releasing current were 40 kV and 40 mA, respectively. The Debye – Scherrer equation was used for the calculation of crystallite size.

$$D = \frac{k\lambda}{\beta \cos\theta}$$

where k is a constant equal to 0.9, λ is the X-ray wavelength, β is the full width at half maximum and θ is the half diffraction angle.

The mass composition of anatase and rutile was determined via relation of peak intensity of anatase (I_A) and rutile (I_R) [21].

$$\text{Anatase} = \frac{0.79I_A}{0.79I_A + I_R}$$

$$\text{Rutile} = \frac{I_R}{0.79I_A + I_R}$$

where I_A is a peak intensity of anatase phase at 25.3° and I_R is a peak intensity of rutile phase at 27.4°.

The morphology and surface structure is investigated by scanning electron microscopy (SEM) (Jeol JSM – 6400).

จุฬาลงกรณ์มหาวิทยาลัย
CHULALONGKORN UNIVERSITY

3.5 Degradation of diuron

The photoeletrocatalytic activities of the titania film was tested by degradation of diuron. Initial diuron concentration was 10 ppm. In this research, two plates of titanium substrates coated with titania (TiO_2/Ti) and used as anode were submerged in 150 ml solution while graphite sheets were used as cathode. After placing electrodes into diuron solution, voltage was applied and UV-A was irradiated. Samples of 1 ml in volume were collected at 30, 60, 90, 120, 150, 180, 240, 300, 360, and 420 minutes of the experimental time. The samples were filtered through 0.22 μm membrane before being analyzed by HPLC (model Class VP, Shimadzu) equipped with C18 column (5 μm, particle size 250 nm x 4.6 mm, Phenomenex Luna). Acetonitrile and water were used as mobile phase in the ratio of 70:30 with the flow rate of 1.5 ml/min. The UV detector was operated at 254 nm. The degradation percentage was calculated based on concentration at the sampling time (C_t) and initial concentration (C_o) as followed.

$$\text{Degradation percentage} = \frac{C_o - C_t}{C_o} \times 100\%$$

จุฬาลงกรณ์มหาวิทยาลัย
Chulalongkorn University

CHAPTER IV

RESULTS AND DISCUSSION

4.1 Characteristics of titania film

Titania coated on titanium was analyzed by scanning electron microscopy (SEM). The SEM images were shown in Figure 4.1.

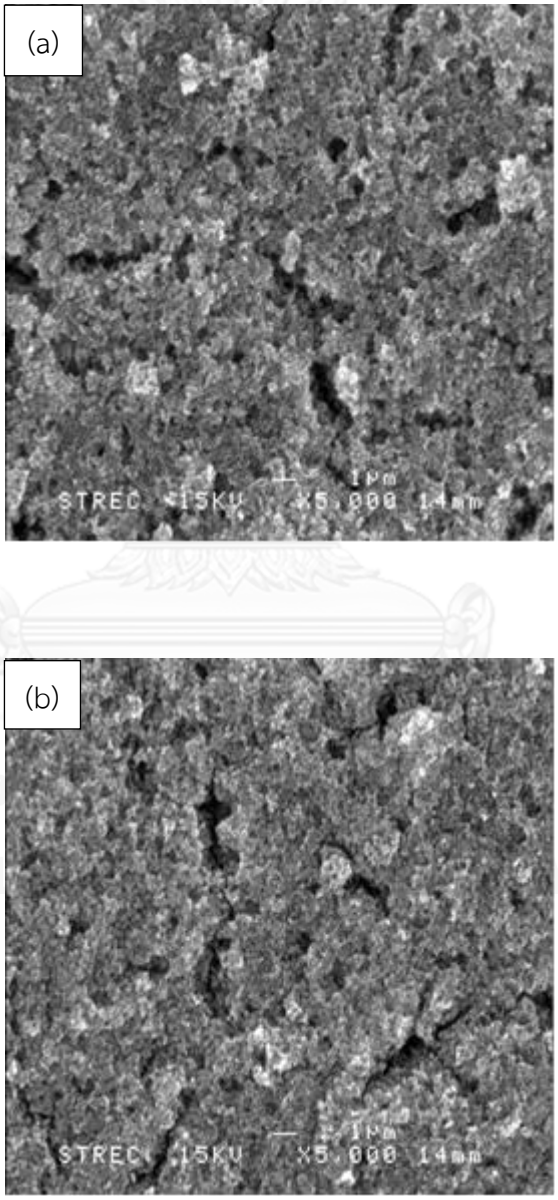

Figure 4.1 SEM images (a) before being calcined 500°C and (b) after being calcined 500°C.

The fingerprint characterization of crystalline of titania was identified using X-ray Diffraction (XRD). Typical XRD diffraction patterns of titania film were shown in Figure 4.2. Anatase phase shows strong peak at 25.3°, 52.9°, and 70.5° meanwhile rutile phase emerges at 27.4°. All peaks were discovered both before and after calcination at 500°C. Intensity peak has change when titania film was calcined. It indicated phase and particle size transformation.

The Debye – Scherrer equation was used for calculation crystalline size on titania film.

$$D = \frac{k\lambda}{\beta \cos\theta}$$

where k is a constant equal to 0.9, λ is the X-ray wavelength, β is the full width at half maximum and θ is the half diffraction angle.

Phase component was determined from relation of peak intensity of anatase (I_A) and rutile (I_R) [21].

$$\text{Anatase} = \frac{0.79I_A}{0.79I_A + I_R}$$

$$\text{Rutile} = \frac{I_R}{0.79I_A + I_R}$$

where I_A is a peak intensity of anatase phase at 25.3° and I_R is a peak intensity of rutile phase at 27.4°.

จุฬาลงกรณ์มหาวิทยาลัย
Chulalongkorn University

The analyzed data was shown in Table 4.1.

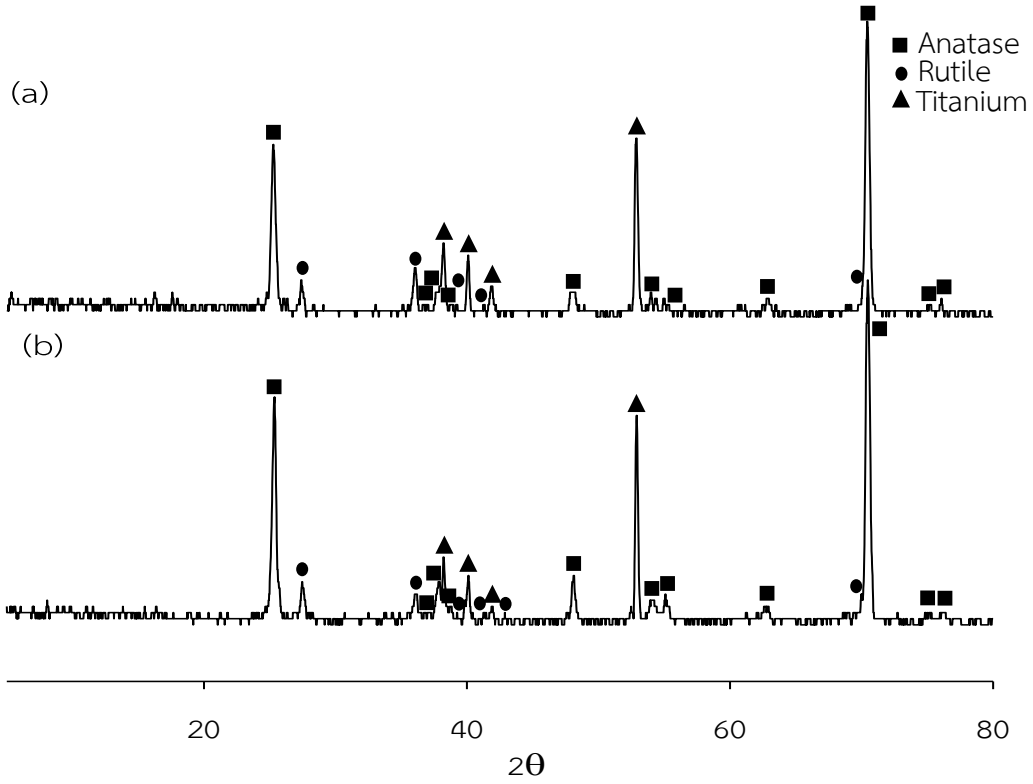

Figure 4.2 XRD patterns of titania film (a) before calcined 500°C and (b) after calcined 500°C.

Crystalline size has grown after film was calcined. It was possibly a result from crystalline structure of titania binder. Moreover, ratio between anatase and rutile phase was changed. Structure of titania binder transformed amorphous to anatase phase after it was calcined at 500°C.

Table 4.1 Crystalline size and phase composition percentage.

Calcination 500°C	Anatase crystalline size (nm)	Mass composition (%)		
		Anatase	Rutile	Ratio
Before calcination at 500°C	76.81	78.05	21.95	3.56
After calcination at 500°C	101.77	84.31	15.69	5.37

4.2 2^k – factorial design

This method was used to determine effect that has impact on experimental observation. Value of parameter was divided into 2 levels (-1 is low level and 1 is high level), as shown in Table 4.2. 2^k - factorial design is considered as preliminary investigation because it used lower number of test run than other techniques. In this study, 3 parameters were considered, i.e., bias potential, pH and anion. The presence of factors influentially affected diuron degradation in photoelectrocatalysis. Therefore, this experimental plan was consisted of 8 test runs. It was shown in Table 4.3 while responses were presented in the same table.

Table 4.2 Factors and levels in 3 factors 2^k - factorial design.

Variables	Symbols	Levels	
		-1	1
Bias potential (V)	X_1	5	10
pH	X_2	3	11
Anion (0.1 M $NaNO_3$), (ml)	X_3	0	5

Table 4.3 The condition and response of test run.

Run	X_1	X_2	X_3	X_1X_2	X_1X_3	X_2X_3	$X_1X_2X_3$	y_i (% diuron degradation)
1	-1	-1	-1	1	1	1	-1	81.22
2	1	-1	-1	-1	-1	1	1	99.71
3	-1	1	-1	-1	1	-1	1	35.85
4	1	1	-1	1	-1	-1	-1	57.04
5	-1	-1	1	1	-1	-1	1	100.00
6	1	-1	1	-1	1	-1	-1	74.13
7	-1	1	1	-1	-1	1	-1	24.99
8	1	1	1	1	1	1	1	68.61

จุฬาลงกรณ์มหาวิทยาลัย
Chulalongkorn University

The experimental data was shown in Table 4.2 that was analysed by empirical model:

$$\hat{y} = \beta_0 + \beta_1 X_1 + \beta_2 X_2 + \beta_3 X_3 + \beta_{12} X_1 X_2 + \beta_{13} X_1 X_3 + \beta_{23} X_2 X_3 + \beta_{123} X_1 X_2 X_3$$

where $\hat{y}$ is response (% diuron degradation at 420 minutes) and β_i, β_{ij}, and β_{ijk} are parameter of explanatory variables that shown in Table 4.4. X_i, X_{ij}, and X_{ijk} are coded independent variables.

Table 4.4 Factor values.

parameter of explanatory variables	Factor value
β_0	67.70
β_1	14.36
β_2	-42.14
β_3	1.52
β_{12}	18.05
β_{13}	-5.48
β_{23}	1.88
β_{123}	16.70

จุฬาลงกรณ์มหาวิทยาลัย
Chulalongkorn University

In Table 4.4, values of β_3, β_{13}, and β_{23} are lower than other parameters. Figure 4.3 shows calculated effects of data in Table 4.4. They are presented in bar graph. β_1 represents for effect of applied voltage. It has positive value. Therefore, the percentage of diuron degradation is increased when the voltage is increased. β_2 represents for effect of pH. It has negative value so that efficiency of the degradation is inversely dependent on pH. Furthermore, value of 2 interaction effects of X_1 and X_2 and 3 interaction effects have influenced to response in high level. As, β_3 (it was effect of anion), value of 2 interaction effects of X_1 and X_3 and 2 interaction

effects of X_2 and X_3 led to response in low level. These are likely non-significant effect. However, they were not eradicated. They were until improved by statistical technique.

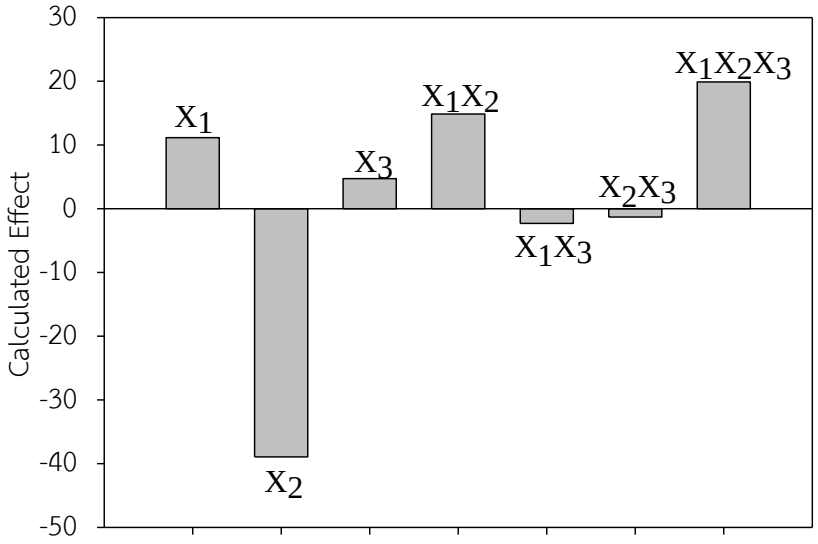

Figure 4.3 Calculated effect bar plot.

Normal probability plot was used for assured non-significant effect. It exhibits 2 non – significant effects since they were nearly zero. β_3, and β_{23} were non – significant effects that it was considered from relation between calculated effect and cumulative probability (P_i). It was shown in Figure 4.4.

จุฬาลงกรณ์มหาวิทยาลัย
Chulalongkorn University

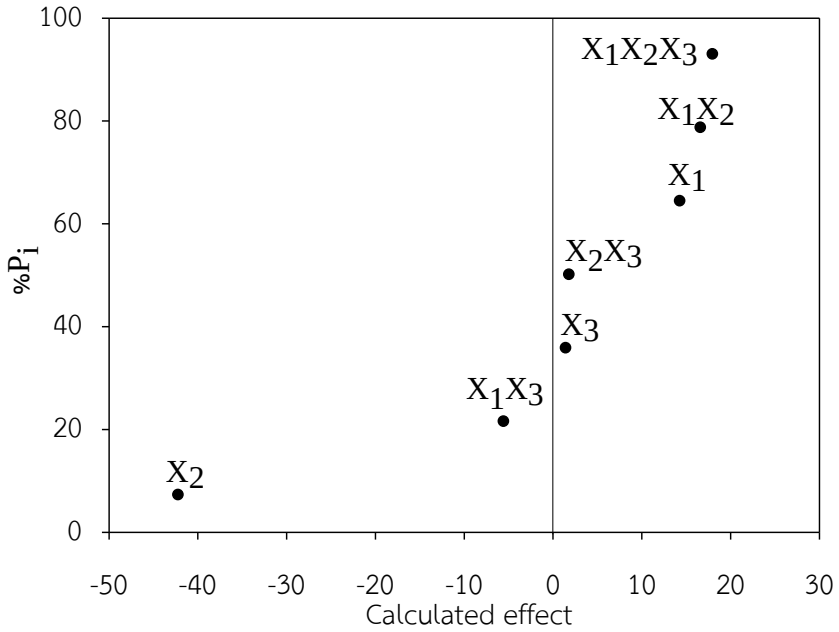

Figure 4.4 Normal probability plots

Precision of calculated effect was second method that it used for find non-significant effect. Three non – significant effects were found plausibly to be zero. As a result, they could be deleted from the experimental model.

The results from both methods identified 3 non-significant effects which were β_3, β_{13}, and β_{23}, corresponding effect of applied voltage, dual effect of pH and applied voltage, and trio relation of anion, pH, and applied voltage.

จุฬาลงกรณ์มหาวิทยาลัย
Chulalongkorn University

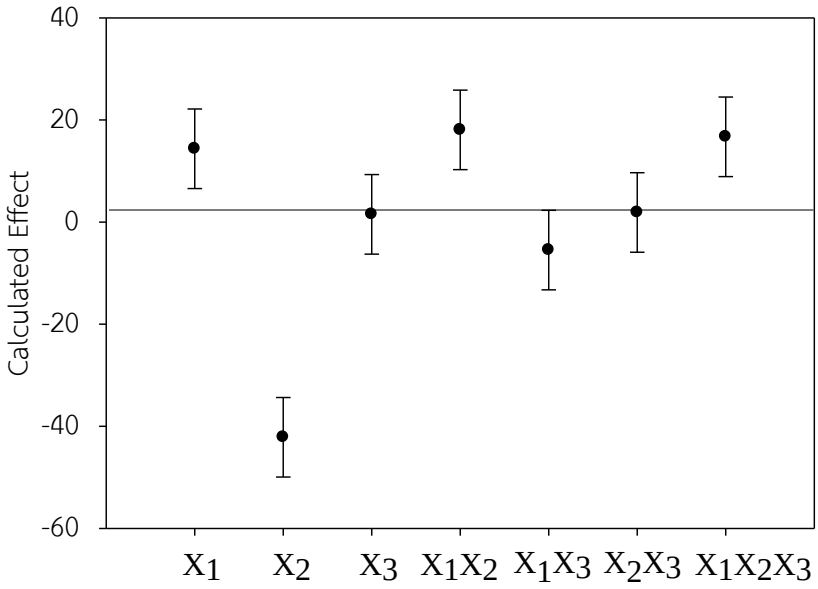

Figure 4.5 Precision of calculated effect.

From the results, it should be noted that nitrate ion can also be enhanced the efficiency of diuron degradation as shown in Figure 4.6 – Figure 4.7. nitrate ion was added into the solution lead to the synergetic effect. The synergetic effect may be occurred when the electron transferred rate increase as a result of direct reduction via electron.

จุฬาลงกรณ์มหาวิทยาลัย
Chulalongkorn University

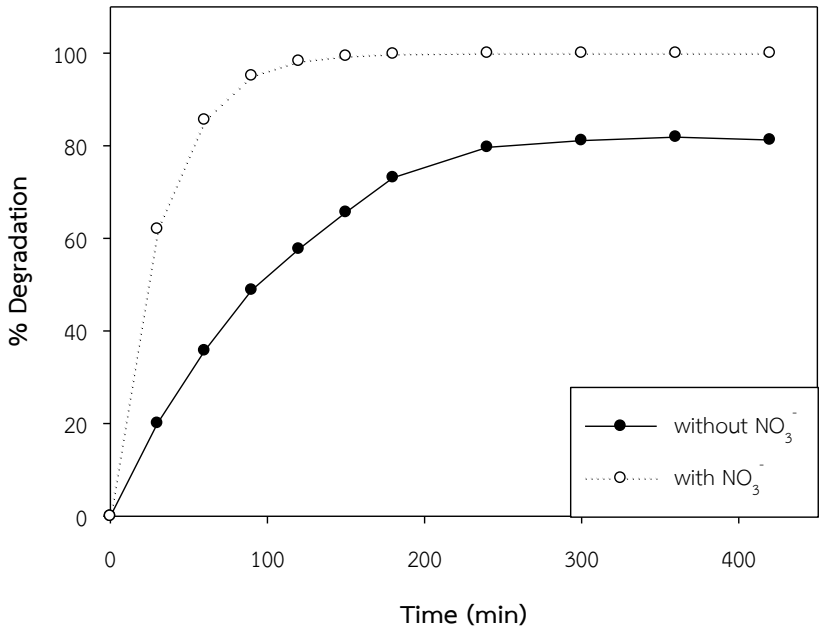

Figure 4.6 Efficiency of the diuron degradation with and without nitrate ion in acidic condition and applied voltage 5 V.

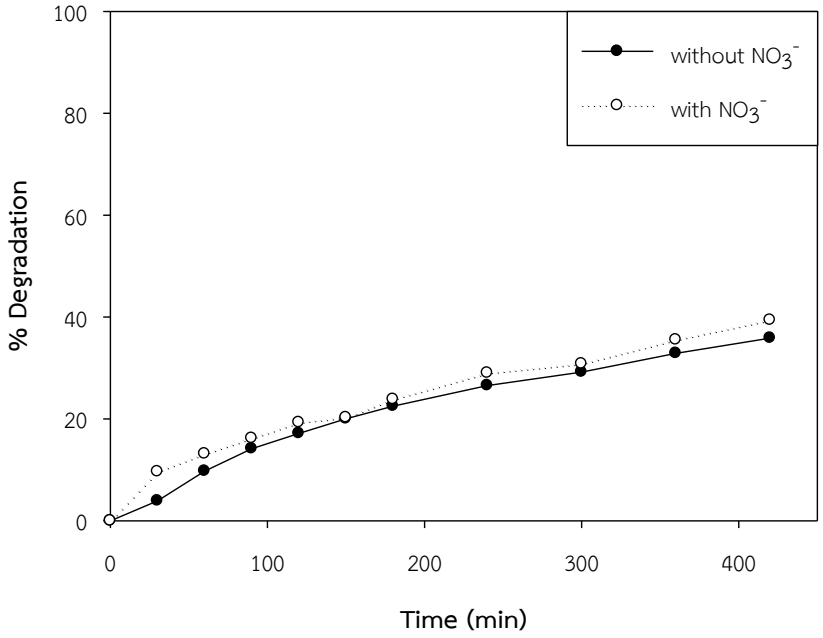

Figure 4.7 Efficiency of the diuron degradation with and without nitrate ion in alkaline condition and applied voltage 5 V.

Previous study, the complete product of diuron degradation was nitrate ion. It represented in equation 4.2.1 [4].

$$C_9H_{10}Cl_2N_2O + 13O_2 \longrightarrow 2HCl + 2HNO_3 + 9CO_2 + 3H_2O \qquad 4.2.1$$

From the result, if the diuron degradation was completely degraded. Nitrate ion was detected. Moreover, nitrate ion reacted to photon and electron and transformed to nitrite ion. Mechanism shows in equation 4.2.2 – 4.2.8.

i. photolysis [22, 23].

$$NO_3^- + H_2O + hv \longrightarrow NO_2\cdot + OH\cdot + OH^- \qquad 4.2.2$$

$$NO_3^- + hv \longrightarrow NO_2^- + O(^3P) \qquad 4.2.3$$

$$NO_2^- + H_2O + hv \longrightarrow NO\cdot + OH\cdot + OH^- \qquad 4.2.4$$

$$NO_2^- + OH\cdot \longrightarrow NO_2\cdot + OH^- \qquad 4.2.5$$

ii. reduction on graphite electrode [24, 25].

$$NO_3^- + H_2O + 2e^- \longrightarrow NO_2^- + 2OH^- \qquad 4.2.6$$

$$2NO_3^- + 6H_2O + 10e^- \longrightarrow N_{2\,(g)} + 12OH^- \qquad 4.2.7$$

$$2NO_2^- + 4H_2O + 6e^- \longrightarrow N_{2\,(g)} + 8OH^- \qquad 4.2.8$$

In order to prove that the diuron degradation is complete, so the amount of nitrate and nitrite ion was measured via uv - spectrometer. Nitrate ion was measured at 220 mn whlie nitrite ion was measured at 543 nm. 50 ppm of Nitrate ion was added in solution for studying rate of nitrate change. In Figure 4.8 – 4.9 represented amount of nitrate ion and nitrite ion, respectively. Nitrate ion does not change so diuron was not completely decomposed. Furthermore, nitrate was not photolysis and reduction because nitrite ion does not generate.

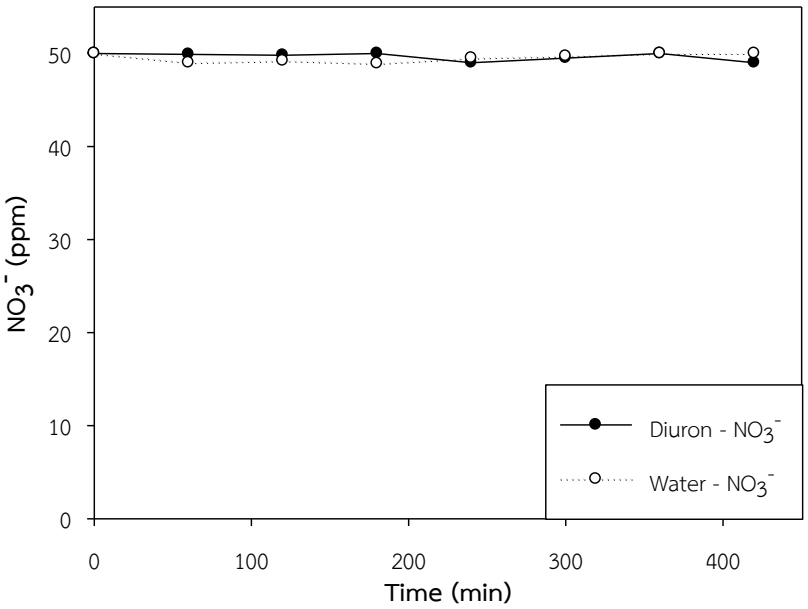

Figure 4.8 Nitrate concentration under pH 7 and applied voltage 0.5 V.

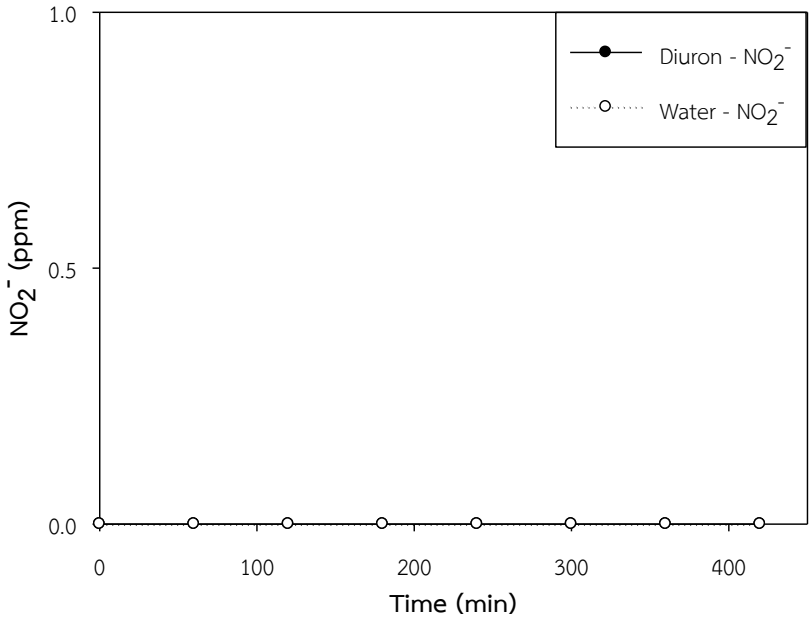

Figure 4.9 Nitrite concentration under pH 7 and applied voltage 0.5 V.

4.3 Effect of applied voltage of diuron degradation

Ordinarily, TiO_2 was excited with photon that has energy higher than band gap energy (3.2 eV). Electron moved from the valence band to the conduction band and hole was generated on TiO_2 surface. It is shown in equation 4.3.1. Water and oxygen react with them and they become hydroxyl radical (OH·) and superoxide radical (O_2^-·), respectively. They are presented in equation 4.3.2 and 4.3.3, respectively. Four reactions occur on TiO_2 surface [2, 6, 26, 27].

$$TiO_2 + h\nu \longrightarrow e_{CB}^- + h^+ \quad 4.3.1$$

$$e_{CB}^- + O_2 \longrightarrow O_2^-\cdot \quad 4.3.2$$

$$h^+ + H_2O \longrightarrow OH\cdot + H^+ \quad 4.3.3$$

$$e_{CB}^- + h^+ \longrightarrow \text{heat} \quad 4.3.4$$

Titania was used as catalyt in the study. It was coated on titanium substrate as film. Compared with particles, titania film commonly has less surface area. The efficiency of catalysis is low. Furthermore, effect of electron – hole recombination is the main reason that decreases efficiency of the catalysis. When electric potential was applied to the system, an electric field was immediately created, leading to electron transfer between the two electrodes. As a result, electron – hole recombination was reduced. The reaction follows equation 4.3.5 – 4.3.13 [18, 20, 28-30].

Anode (TiO_2/Ti):

$$TiO_2 + h\nu \longrightarrow e_{CB}^- + h^+ \quad 4.3.5$$

$$h^+ + H_2O \longrightarrow OH\cdot + H^+ \quad 4.3.6$$

$$OH^- + h^+ \longrightarrow OH\cdot \quad 4.3.7$$

Chulalongkorn University

Cathode (Graphite)

$$e_{CB}^{-} + O_2 \longrightarrow O_2^{-}\cdot \quad 4.3.8$$

$$2e_{CB}^{-} + O_2 + 2H^{+} \longrightarrow H_2O_2 \quad 4.3.9$$

$$O_2^{-}\cdot + H_2O_2 \longrightarrow OH^{-} + OH\cdot + O_2 \quad 4.3.10$$

$$O_2^{-}\cdot + H^{+} \longrightarrow OH_2\cdot \quad 4.3.11$$

$$H_2O_2 + e_{CB}^{-} \longrightarrow OH^{-} + OH\cdot \quad 4.3.12$$

$$H_2O_2 + h\nu \longrightarrow 2OH\cdot \quad 4.3.13$$

Level of applied voltage was studied in this content. It affected the degradation. Voltage was applied in the range of 2.5 V – 10 V. If voltage was higher than 10 V. Bubble appeared on electrodes, which indicated dissociation of water. Water underwent water splitting reaction instead of oxidation. The water was separated into hydrogen and oxygen instead of preforming a reaction with holes and subsequently created hydroxyl radical. Efficiency of degradation was increased when voltage was increased. However, efficiency of degradation was decreased when applied voltage was 10 V. It is shown in Figure 4.10. It was observed that the degradation under the applied voltage of 7.5 V was the highest, i.e., 78.21% within 7 hours. This observation is in agreement with the previous report by Li et al [31, 32].

จุฬาลงกรณ์มหาวิทยาลัย
Chulalongkorn University

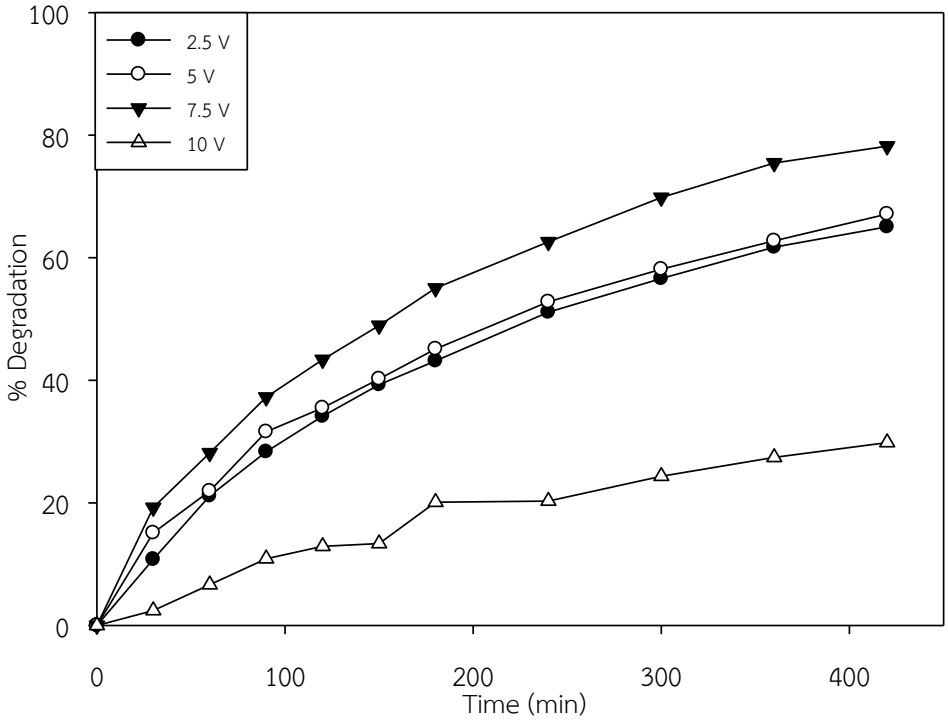

Figure 4.10 Effect of applied voltage for diuron degradation.

Although the applied voltage promoted the degradation of diuron by photoelectrocatalytic method, excess applied voltage dropped diuron degradation efficiency because electron flux was interrupted. Electrons were expelled swiftly from anode leading to electrode corrosion [33, 34]. When applying low voltage to electrodes, electrons which were excited from valence band would instantaneously undergo recombination with holes resulted from insufficient current density in electron induction. This phenomenon is chemical short circuit [14].

According to other authors, kinetic of the photoelectrodegradation of organic pollutants were described by the pseudo-first order kinetics.

$$r = -\frac{dC}{dt} = k_r KC = k_{app} C \qquad 4.3.9$$

where r is the rate of diuron degradation, C is the concentration of the diuron being degraded, t is the irradiation time, and k_{app} is the apparent rate constant of a pseudo first order model. For batch operation, equation 4.3.9 was transformed to equation 4.3.10 when C_0 is an initial concentration of diuron.

$$\ln \frac{C_0}{C} = k_{app}t \qquad 4.3.10$$

This model was used to describe kinetic study of diuron degradation. The apparent rate constants combined overall rate constants in system. From this relation, the apparent rate constants can be found. The results are shown in Figure 4.11. They were determined from slope of equation 4.3.10. The apparent rate constants were shown in Table 4.4.

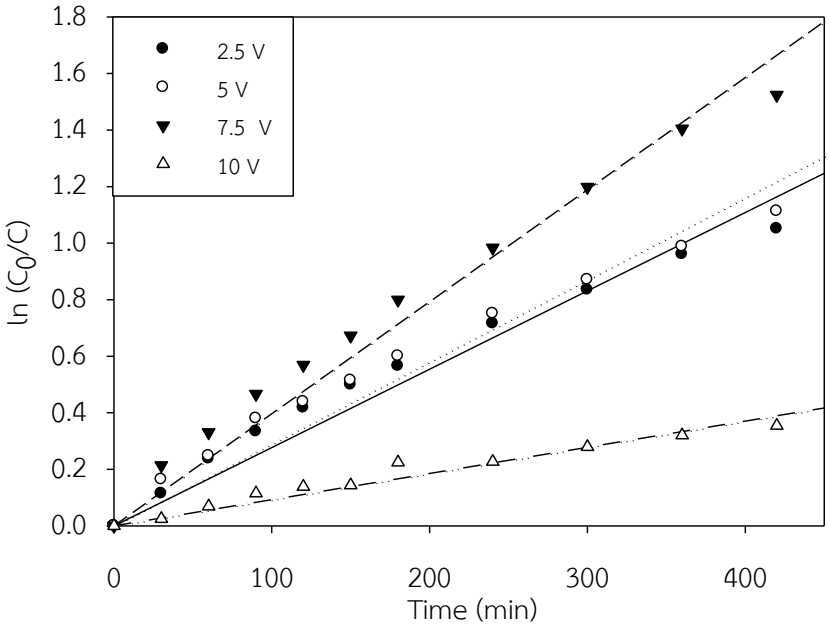

Figure 4.11 First – order linear transforms plot of the photoelectrocatalytic degradation at pH 7.

The apparent rate constants are show in Table 4.5. Both before and after 120 minute, the kinetics of diuron degradation could still be represented by the pseudo-first order equation. Moreover, the apparent rate constants of electrolysis were used to compare value of the apparent rate constants of photoelectrocatalysis. They presented behavior of diuron degradation. The apparent rate constants of photoelectrocatalysis are higher than that obtained from electrolytic reaction. They exhibited prominence. The apparent rate constants were displayed in Table 4.6. The apparent rate constants of 2.5 V – 7.5 V have increase from electrolysis but the apparent rate constants of 10 V has equal to electrolysis. It justified theories. If the

voltage was applied in system higher than optimal voltage, efficiency of degradation decreased. The optimal voltage depends on many factors such as type of recalcitrant organic pollutant, size and type of electrode.

Table 4.5 The apparent rate constants of photoelectrocatalysis at pH 7.

Voltage (V)	k_{app} (min^{-1}) 120 min	R^2	k_{app} (min^{-1}) 420 min	R^2
2.5	0.0036	0.9930	0.0028	0.9588
5	0.0039	0.9672	0.0029	0.9490
7.5	0.0051	0.9687	0.0040	0.9699
10	0.0012	0.9844	0.0009	0.9522

Table 4.6 The apparent rate constants of electrolysis at pH 7.

Voltage (V)	k_{app} (min^{-1}) 120 min	R^2	k_{app} (min^{-1}) 420 min	R^2
2.5	0.0007	0.7957	0.0013	0.9560
5	0.0009	0.9123	0.0007	0.8201
7.5	0.0014	0.9077	0.0010	0.9389
10	0.0015	0.9746	0.0009	0.8101

Furthermore, diuron was detected by HPLC. Products of diuron degradation were detected. These results were represented in Figure 4.12 – 4.15. However, these intermediates cannot be identified because of the lack of standard references.

However, number of intermediates was found. Diuron degradation is consisted of many pathways and may influence apparent rate constants. Intermediates were found approximately at retention time of 1.7, 1.9, 2.3, 2.4, 2.6, 2.7, and 3.8 minute. These intermediates may be products in main pathway of the degradation. Intermediates were investigated. They increased when diuron was degraded. Moreover, at the applied voltage at 7.5 V, all intermediates product which had the retention time lower than 1.3 minute was found whereas only 10 kinds of intermediates was detected when applying the voltage of 10 V. This might be the result from the differences in degradation pathways in case of changing applied potential.

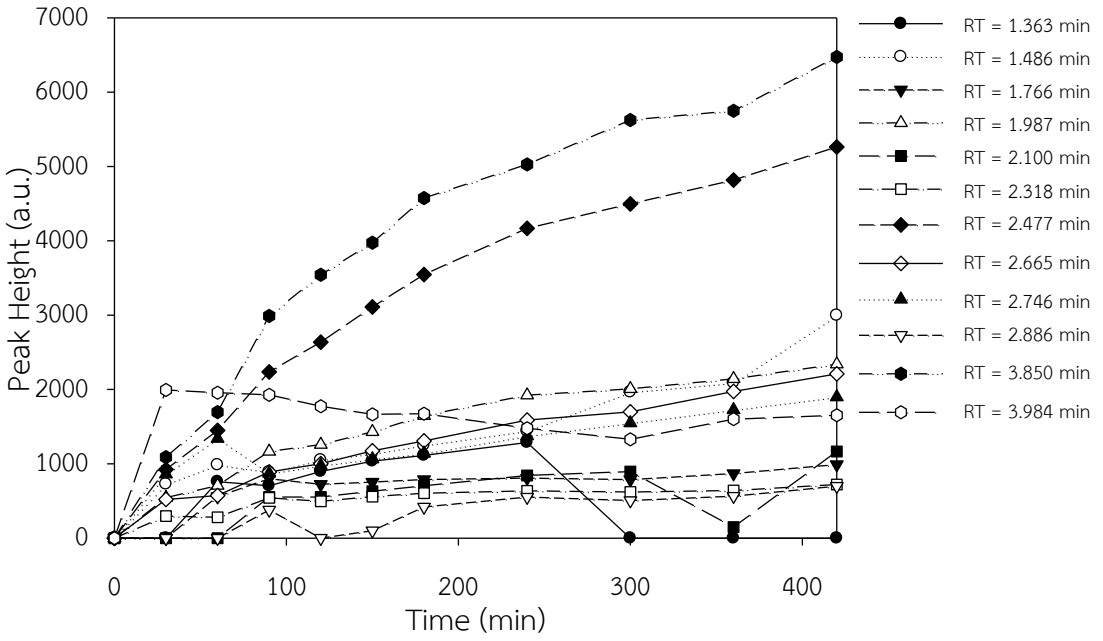

Figure 4.12 HPLC peak height of intermediates generated during photoelectrocatalytic degradation of diuron at applied voltage 2.5 V.

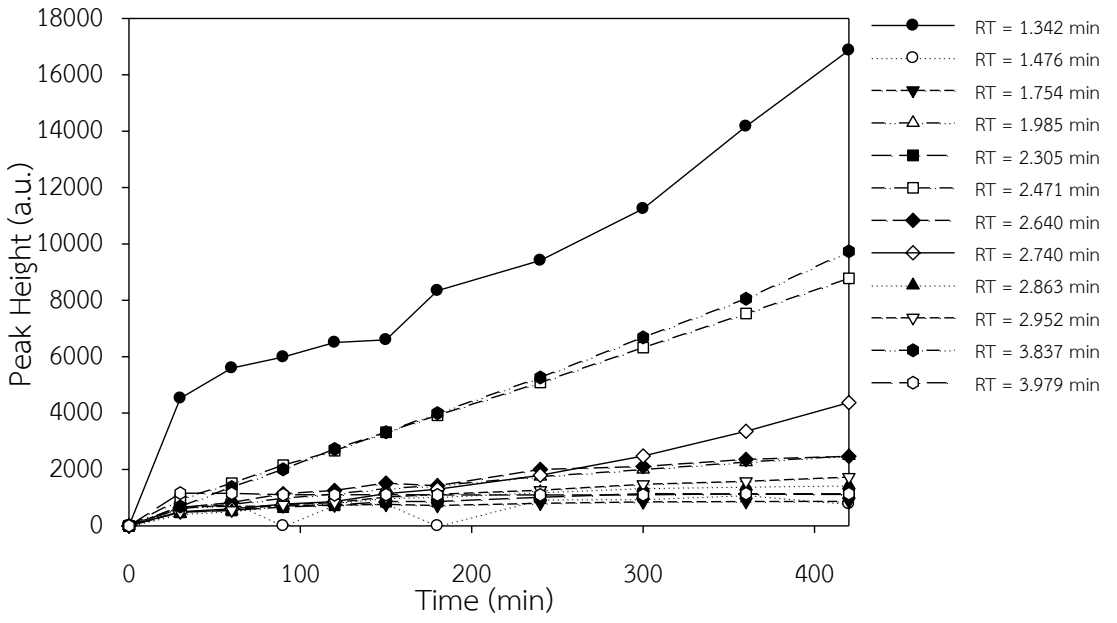

Figure 4.13 HPLC peak height of intermediates generated during photoelectrocatalytic degradation of diuron at applied voltage 5 V.

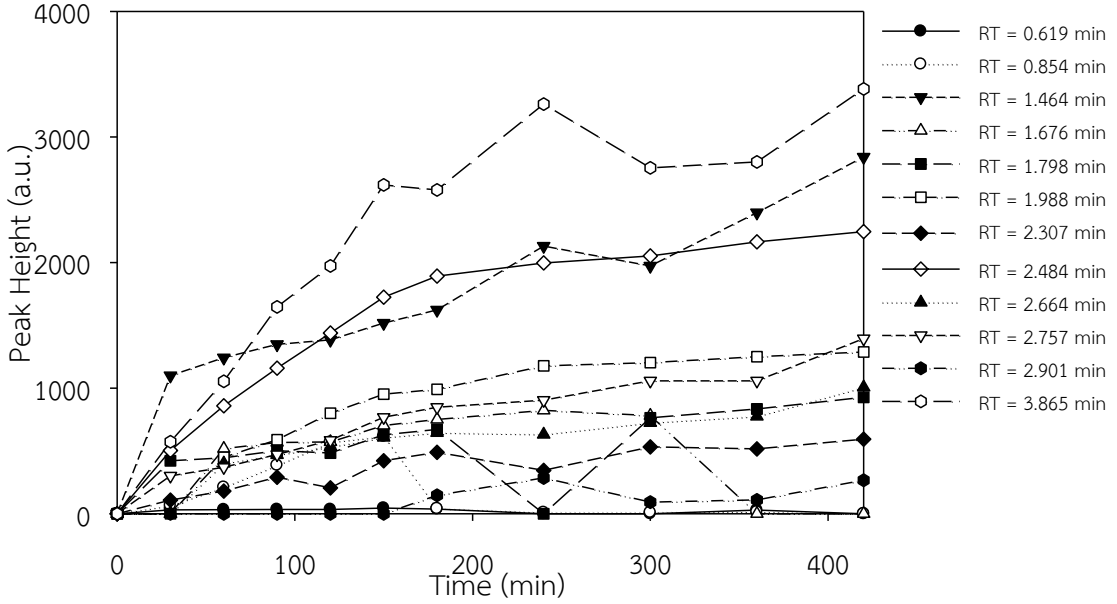

Figure 4.14 HPLC peak height of intermediates generated during photoelectrocatalytic degradation of diuron at applied voltage 7.5 V.

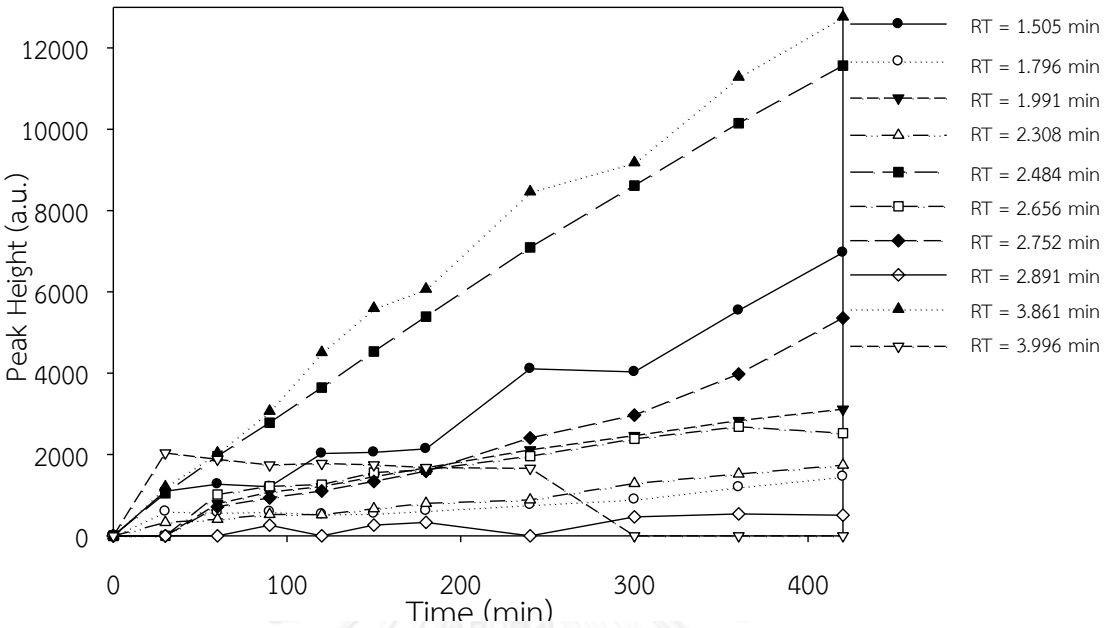

Figure 4.15 HPLC peak height of intermediates generated during photoelectrocatalytic degradation of diuron at applied voltage 10 V.

4.4 Effect of pH and applied voltage of diuron degradation

When pH of solution is changed, charge on surface of titania is modified. The charge on surface is positive when the the point of zero charge (pH_{pzc}) is higher than pH value. Negative charge appears on titania surface when the pH_{pzc} is lower. The pH_{pzc} for titania is approximately 6 [20]. These are represented in equation 4.4.1 – 4.4.2 [29]. Moreover, pH affects the ionization state of the organic pollutants.

Acidic condition ($pH < pH_{pzc}$)

$$TiOH + H^{+} \longrightarrow TiOH_2^{+} \qquad 4.4.1$$

Alkaline condition ($pH > pH_{pzc}$)

$$TiOH + OH^{-} \longrightarrow TiO^{-} + H_2O \qquad 4.4.2$$

Efficiency of degradation was enhanced or decreased due to the interaction force between pollutant and titania. Each of organic compounds requires different

pH for degradation. For example, Rhodamine B was highly decolorized in alkaline condition [35], 4,4' – oxydianiline was demineralized with an acidic condition [20]. On the other hand 4 – chlorophenol shows high efficiency of degradation under both conditions [36]. Diuron was indicated by this result. It was greatly degradated at low pH, as shown in Figure 4.16.

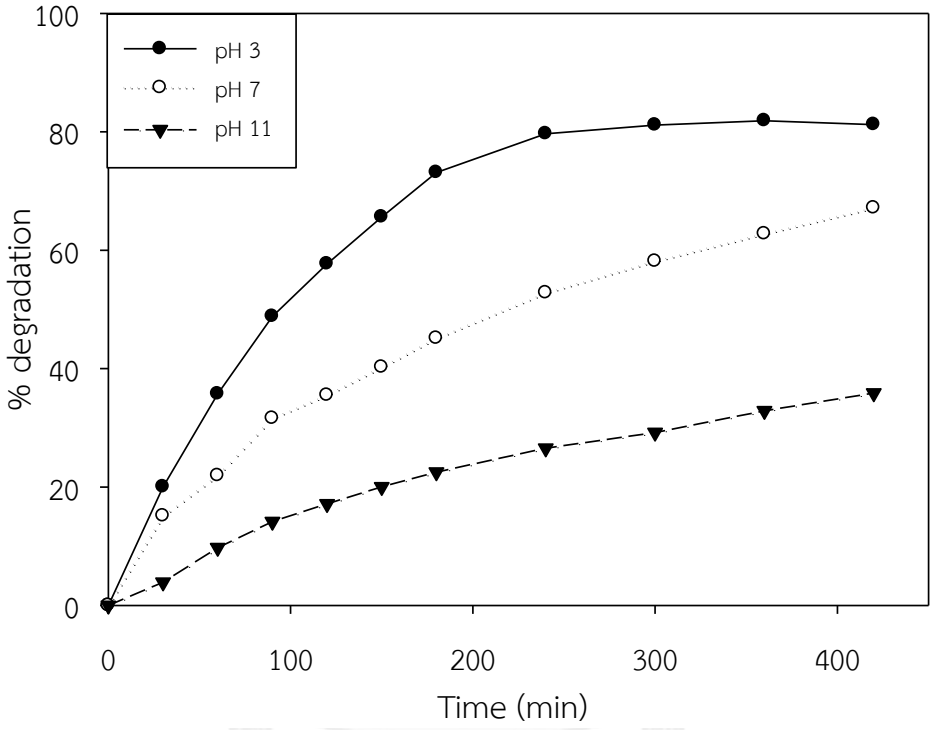

Figure 4.16 Effect of pH for diuron degradation under applied voltage 5 V.

There were 3 reasons contributing to the degradation of pollutants in photoelectrocatalysis [14].

i. direct photo – reduction by electrons (e^-_{CB}).

ii. direct photo – oxidation by holes (h^+).

iii. direct react of hydroxyl radicals (OH·).

Results from the experimental are in agreement with previous research. Major reaction was oxidation via holes. It is due to the different charges between diuron and titania, thus, the probability of adsorption of diuron on titania surface is

increased. As in Table 4.7, rate of diuron degradation in acidic condition is almost 100% increase from the rate at pH 7 while in alkaline condition, efficiency of diuron degradation is about 50% decreased.

Table 4.7 The apparent rate constants of photoelectrocatalysis under applied voltage of 5 V.

pH	k_{app} (min^{-1}) 120 min	R^2	k_{app} (min^{-1}) 420 min	R^2
3	0.0073	0.9991	0.0052	0.8042
7	0.0039	0.9672	0.0029	0.9490
11	0.0016	0.9919	0.0010	0.9351

When, external energy was applied. It affected to demineralization. Diuron degradation is increased when potential voltage is increased. It represented increasing separation of electrons leading to creative many holes on surface of titania. Effect of both pH and applied voltage supported each other. This synergistic effect was expected to be the result from the inhibition of electron/hole recombination by the applied potential. This result was displayed in Figure 4.17.

On the other hand, effect of applied potential and pH could be described by the kinetic. The rate of degradation was high under acidic and large applied voltage. The pseudo – first order equation cannot effectively predict diuron degradation rate after 120 minutes because degradation rate may be affected by the intermediate components in system. This equation was better predicted under alkaline condition. These were shown in Figure 4.18 – 4.19 and Table 4.8 – 4.11.

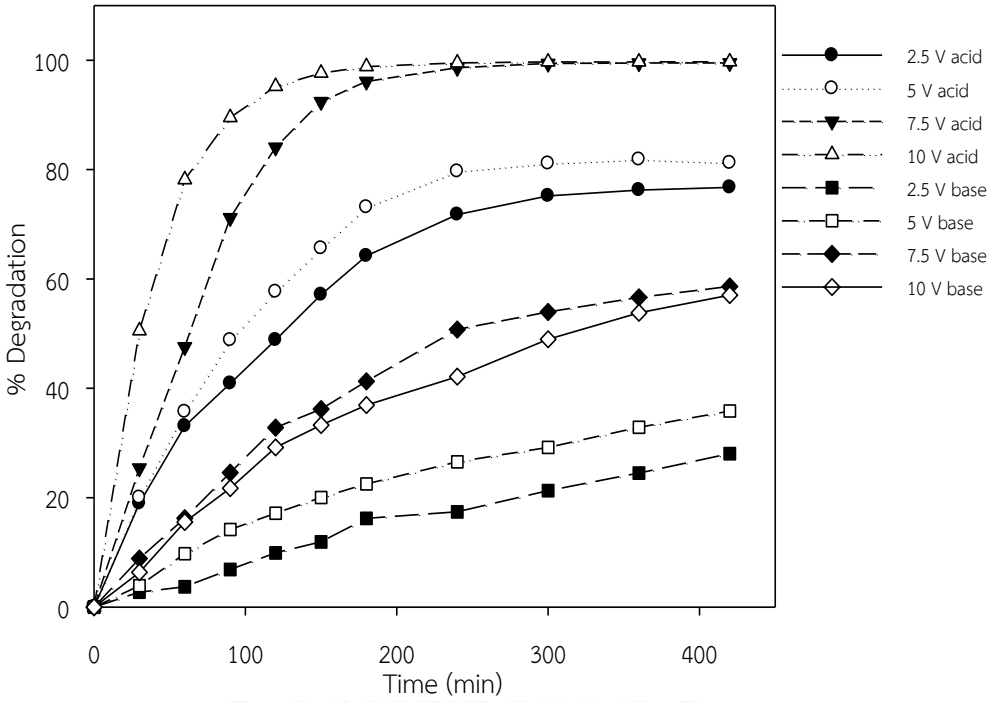

Figure 4.17 Effect of pH for diuron degradation under various applied voltage.

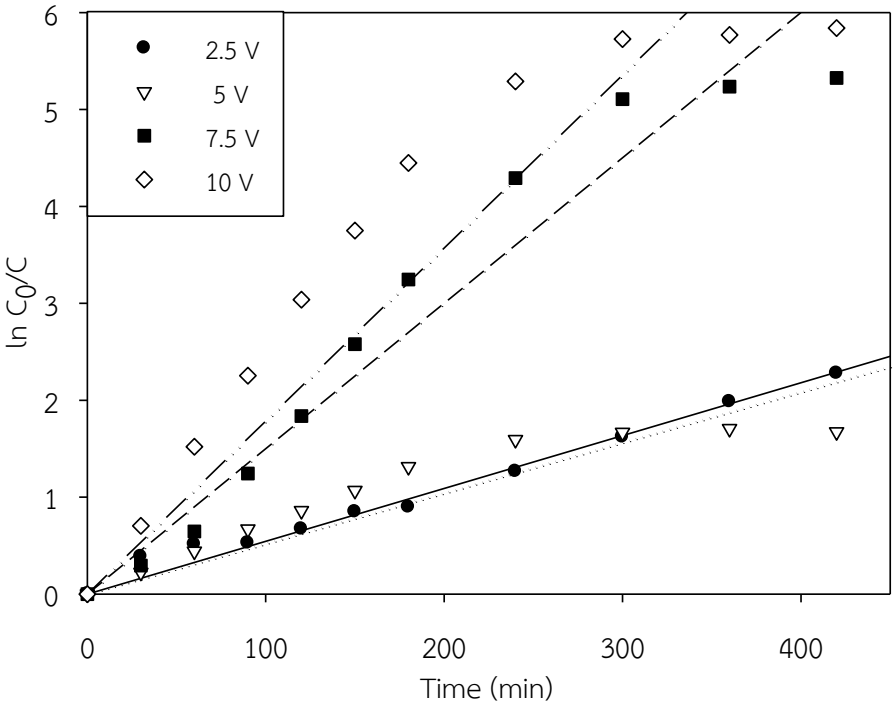

Figure 4.18 First – order linear transforms plot of the photoelectrocatalytic degradation at pH 3.

Table 4.8 The apparent rate constants of photoelectrocatalysis at pH 3.

Voltage (V)	k_{app} (min^{-1}) 120 min	R^2	k_{app} (min^{-1}) 420 min	R^2
2.5	0.0055	0.9110	0.0055	0.9810
5	0.0073	0.9991	0.0052	0.8042
7.5	0.0141	0.9641	0.0150	0.9446
10	0.0252	0.9995	0.0179	0.8142

Table 4.9 The apparent rate constants of electrolysis at pH 3.

Voltage (V)	k_{app} (min^{-1}) 120 min	R^2	k_{app} (min^{-1}) 420 min	R^2
2.5	0.0026	0.9977	0.0021	0.8668
5	0.0040	0.9956	0.0032	0.9747
7.5	0.0020	0.8594	0.0025	0.9603
10	0.0018	0.8812	0.0023	0.9769

จุฬาลงกรณ์มหาวิทยาลัย
Chulalongkorn University

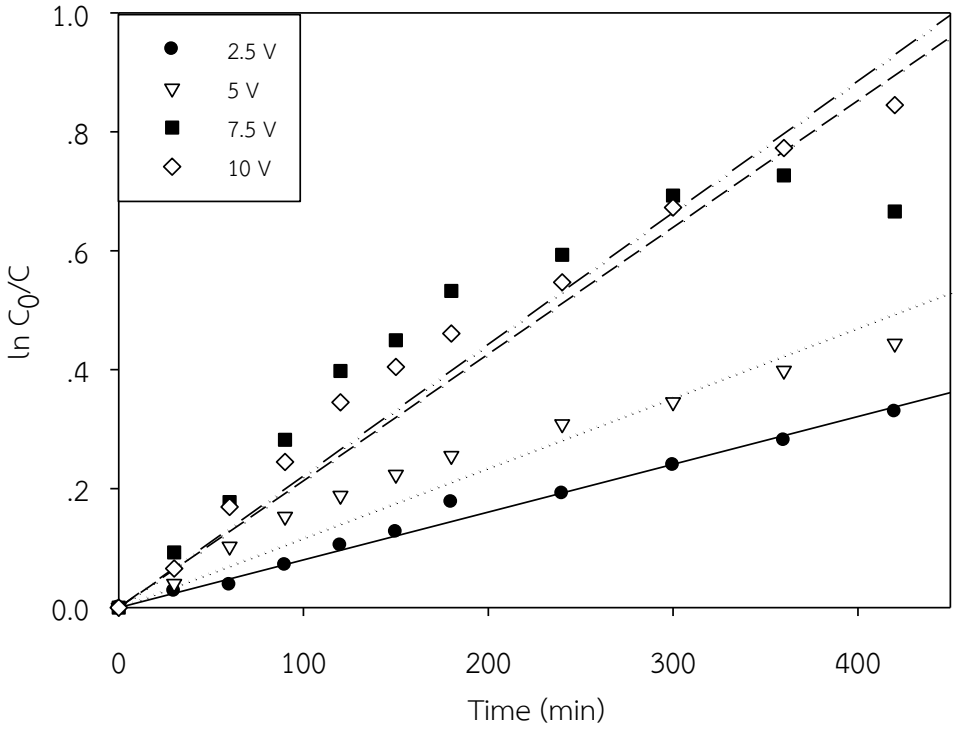

Figure 4.19 First – order linear transforms plot of the photoelectrocatalytic degradation at pH 11.

Table 4.10 The apparent rate constants of photoelectrocatalysis at pH 11.

Voltage (V)	k_{app} (min^{-1}) 120 min	R^2	k_{app} (min^{-1}) 420 min	R^2
2.5	0.0008	0.9728	0.0008	0.9881
5	0.0016	0.9919	0.0012	0.9351
7.5	0.0032	0.9954	0.0021	0.7883
10	0.0028	0.9938	0.0022	0.9657

จุฬาลงกรณ์มหาวิทยาลัย
Chulalongkorn University

Table 4.11 The apparent rate constants of electrolysis at pH 11.

Voltage (V)	k_{app} (min^{-1}) 120 min	R^2	k_{app} (min^{-1}) 420 min	R^2
2.5	0.0027	0.9964	0.0020	0.9454
5	0.0026	0.9954	0.0020	0.9454
7.5	0.0014	0.9927	0.0013	0.9941
10	0.0014	0.9077	0.0010	0.9389

Figure 4.20 – 4.22 presented signals of intermediates. In acidic condition, more intermediates were detected when compared with intermediates which were generated in alkaline condition. Due to diuron was degraded with high efficiency, more intermediate compounds were formed. The results were shown in Figure 4.17. Moreover, as seen in Figure 4.20 – 4.23, there was more intermediate formed when the applied voltage was increased. At this condition, intermediates were found at retention time of 1.47, 1.75, 2.09, 3.80 and 4.77 minute, respectively. However, at applied voltage higher than 5 V, intermediates were found at retention time of 0.37, 2.32, 2.64, and 4.18 minute. Therefore, the aforementioned results of intermediate found at various retention times showed that the degradation had different pathway when the applied voltage was changed. In alkaline condition, trend of intermediate formed is as same as in acidic condition but intermediates were found at retention time of 0.63, 1.72, 1.98, 2.46, 2.63, 2.73, 3.82 and 4.08 minute instead. The previous results were shown in Figure 4.24 – 4.27.

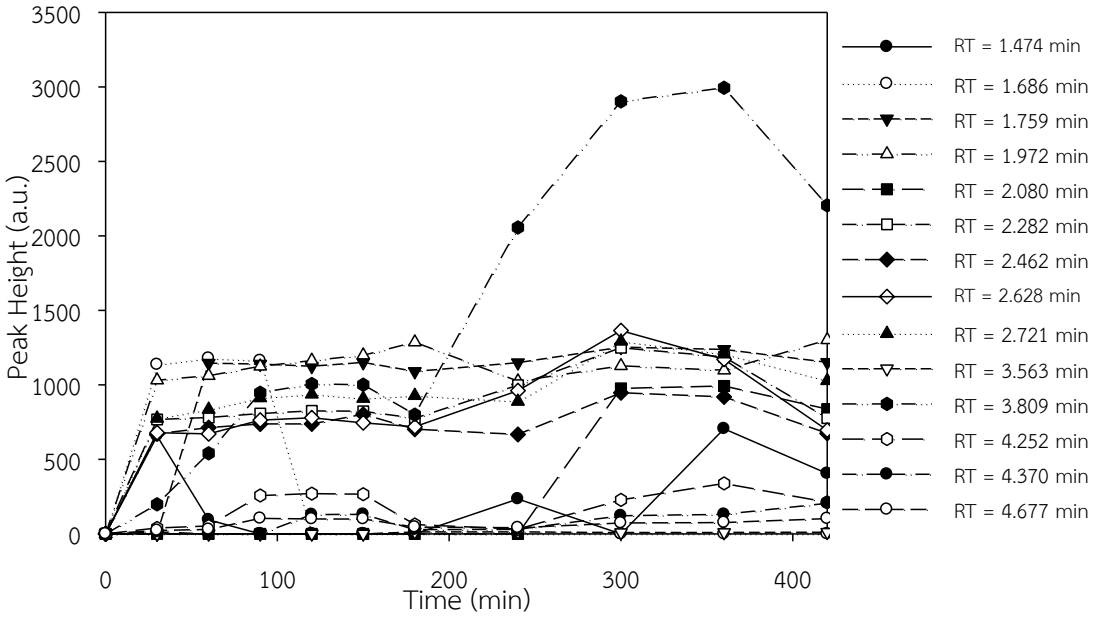

Figure 4.20 HPLC peak heights of intermediates generated during photoelectrocatalytic degradation of diuron under pH 3 and applied voltage 2.5 V.

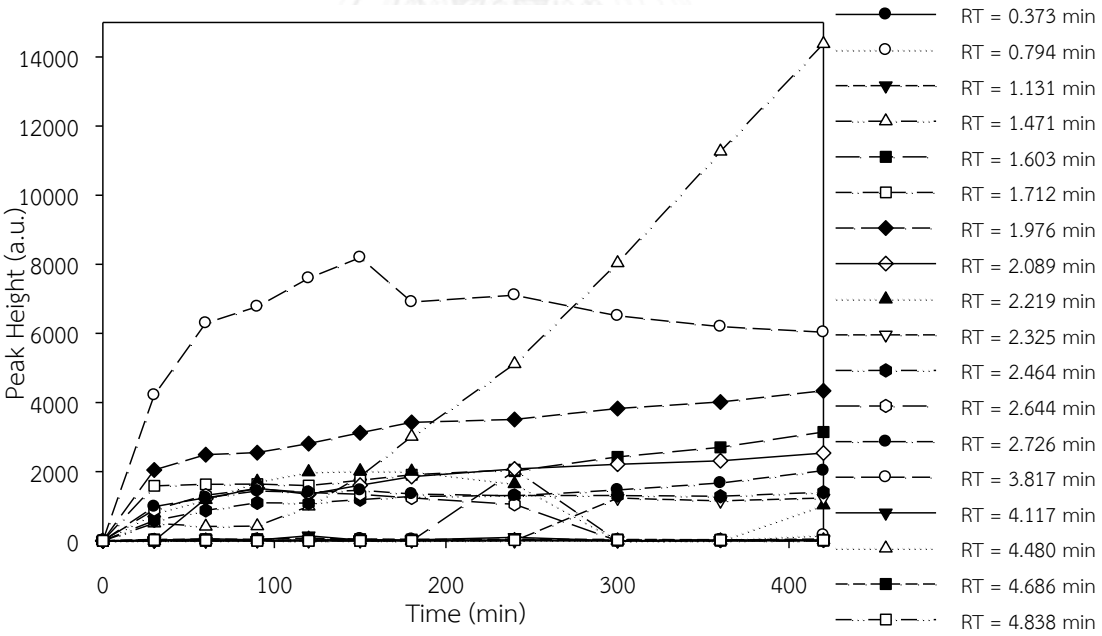

Figure 4.21 HPLC peak heights of intermediates generated during photoelectrocatalytic degradation of diuron under pH 3 and applied voltage 5 V.

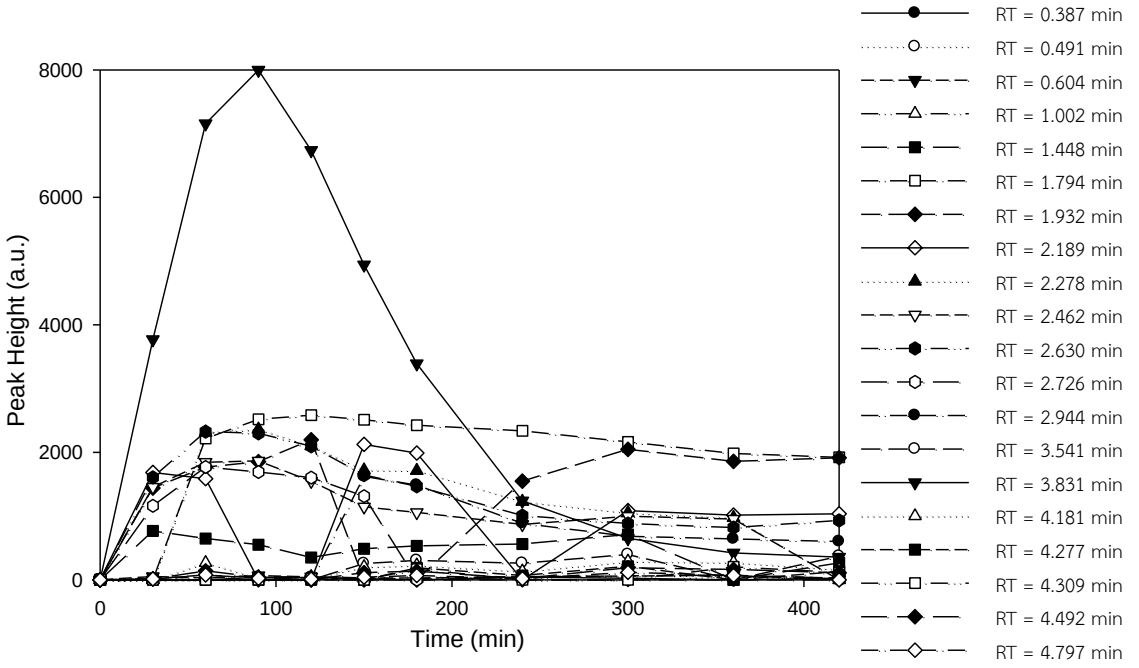

Figure 4.22 HPLC peak heights of intermediates generated during photoelectrocatalytic degradation of diuron under pH 3 and applied voltage 7.5 V.

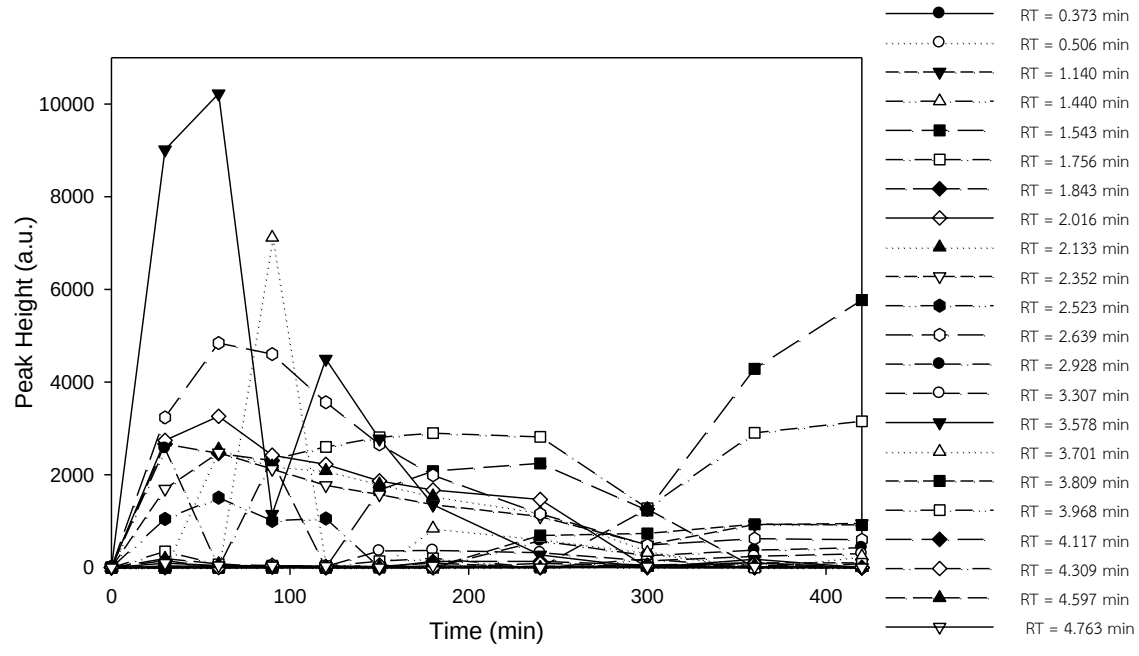

Figure 4.23 HPLC peak heights of intermediates generated during photoelectrocatalytic degradation of diuron under pH 3 and applied voltage 10 V.

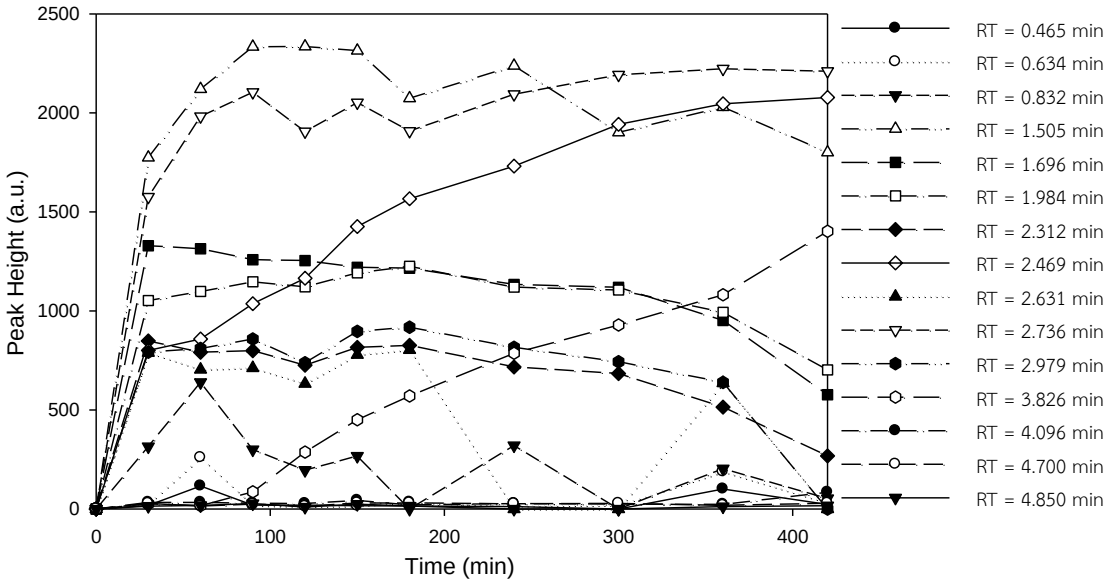

Figure 4.24 HPLC peak heights of intermediates generated during photoelectrocatalytic degradation of diuron under pH 11 and applied voltage 2.5 V.

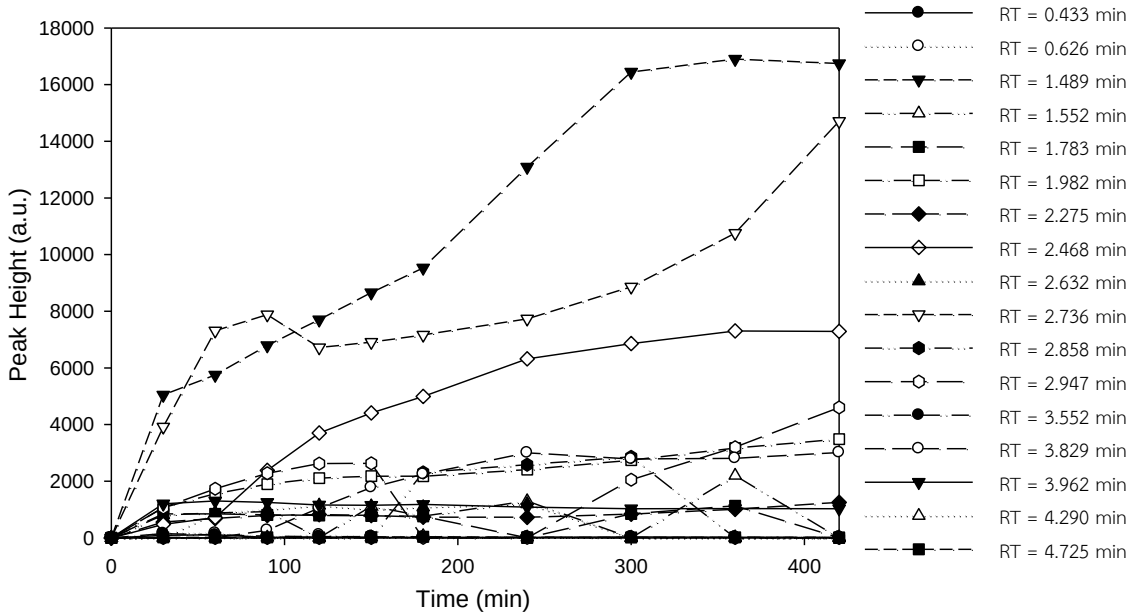

Figure 4.25 HPLC peak heights of intermediates generated during photoelectrocatalytic degradation of diuron under pH 11 and applied voltage 5 V.

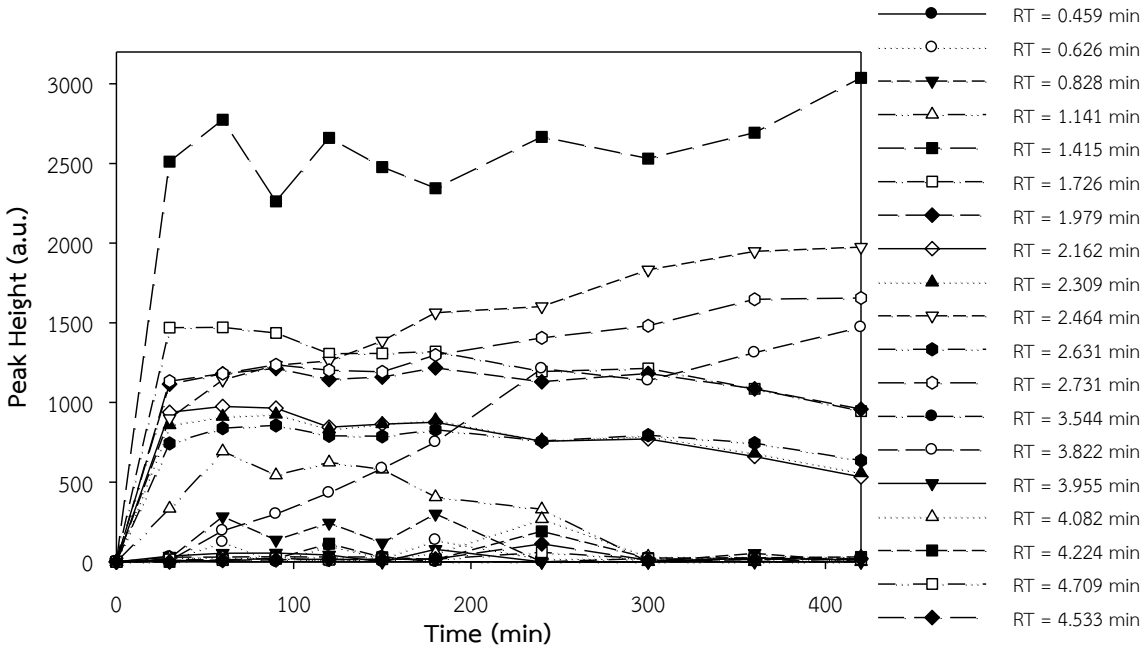

Figure 4.26 HPLC peak heights of intermediates generated during photoelectrocatalytic degradation of diuron under pH 11 and applied voltage 7.5 V.

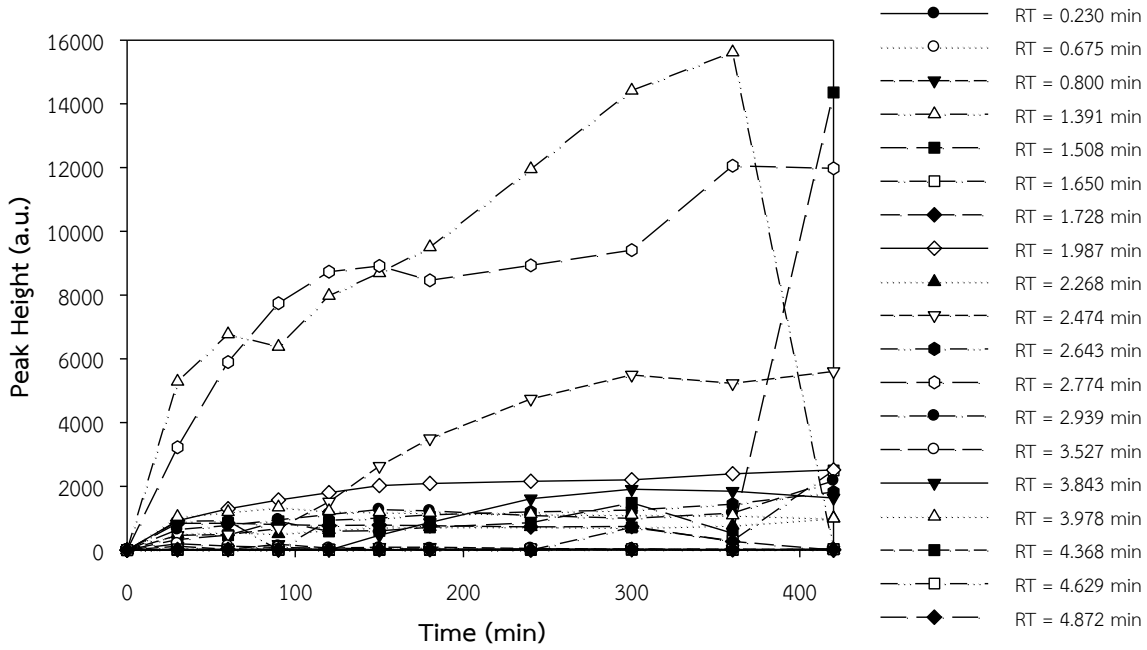

Figure 4.27 HPLC peak heights of intermediates generated during photoelectrocatalytic degradation of diuron under pH 11 and applied voltage 10 V.

4.5 Effect of applied voltage, pH, and chloride ion on diuron degradation

This topic described 3 parameters that affected diuron degradation. Chloride ion (Cl^-) was added in diuron solution. It enhances conductivity of the solution that improves electron transfer rate. Electrons generated via photoelectrocatalytic reaction could be directly reacted with organic compound. It will alter efficiency of diuron degradation. Chloride ion presented behavior like organic pollutant. Mechanisms were shown in equations 4.4.1 – 4.4.5. Chloride ion was transformed to radical in equation 4.4.1 and 4.4.5. It attacked organic pollutants.

i. direct photo – oxidation by holes (h^+).

$$Cl^- + h^+ \longrightarrow Cl\cdot \qquad 4.4.1$$

$$2Cl^- + 2h^+ \longrightarrow Cl_2 + e^- \qquad 4.4.2$$

$$Cl_2 + H_2O \longrightarrow HClO + H^+ + Cl^- \qquad 4.4.3$$

$$HCl \longrightarrow ClO^- + H^+ \qquad 4.4.4$$

ii. direct react of hydroxyl radicals (OH·).

$$Cl\text{-} + OH\cdot \longrightarrow OHCl\cdot^- \qquad 4.4.5$$

Overview of content was demonstrated by statistical technique. It was easy to study the effect of parameters on diuron degradation. The Response surface methodology (RSM) was commonly used to study the effect of parameter that employed multivariate method. Box – Behnken design (BBD) was used for described optimal condition. It was almost rotatable and available for more factors. The Design – Expert 9.0 was used for assisting the calculation RSM – BBD. This software was developed by Stas – Ease Incorporation.

This method determined relationship of effect that has impact to experimental data. Value of parameter was divided into 3 levels (-1 was low level, 0 was central level, and 1 was high level), as shown in Table 4.12. Hence, this rotatable experimental plan was consisted of 15 test runs. It was shown in Table 4.13 while responses were exhibited in the same table.

Table 4.12 Factors and levels in the three – factors three – levels BBD design

Variables	Symbols	Levels		
		-1	0	1
Chloride ion (ppm)	A	250	625	1000
pH	B	3	7	11
Applied voltage (V)	C	0.5	2.5	4.5

The experimental data was shown in Table 4.13. They were inspected by empirical model:

$$\hat{y} = \beta_0 + \beta_1 A + \beta_2 B + \beta_3 C + \beta_{12} AB + \beta_{13} AC + \beta_{23} BC + \beta_{11} A^2 + \beta_{22} B^2 + \beta_{33} C^2$$

where $\hat{y}$ is response and β_i, β_{ij}, and β_{ii} are parameter of explanatory variables that shown in Table 4.13. A, B, and C was coded independent variables.

จุฬาลงกรณ์มหาวิทยาลัย
Chulalongkorn University

Table 4.13 Design of BBD and responses.

Run	A	B	C	Diuron degradation (%)		k_{app} (min^{-1}) 120 min	
				Experimental	Predicted	Experimental	Predicted
1	-1	-1	0	84.83	86.83	0.0069	0.0074
2	-1	1	0	70.65	72.37	0.0034	0.0061
3	1	-1	0	99.90	98.18	0.0189	0.0162
4	1	1	0	60.25	58.25	0.0036	0.0031
5	0	-1	-1	82.01	83.17	0.0068	0.0086
6	0	-1	1	91.90	90.46	0.0092	0.0096
7	0	1	-1	50.47	51.91	0.0012	0.0009
8	0	1	1	68.48	67.32	0.0044	0.0030
9	-1	0	-1	74.59	71.43	0.0052	0.0036
10	1	0	-1	66.46	67.02	0.0043	0.0052
11	-1	0	1	80.33	79.77	0.0048	0.0039
12	1	0	1	78.24	81.40	0.0059	0.0082
13	0	0	0	79.68	79.40	0.0053	0.0054
14	0	0	0	79.07	79.40	0.0058	0.0054
15	0	0	0	79.45	79.40	0.0052	0.0054

The mathematical model was used to represent diuron degradation percentage:

$$\hat{y} = 79.40 - 0.69A - 13.60B + 5.68C - 6.37AB + 1.51AC + 2.03BC + 0.60A^2 - 1.09B^2 - 5.09C^2$$

According to the mathematical model expressed above, it indicates that the pH level is the most influential factor in this study. It presented major effect of diuron degradation. Whereas, the analysis of variance (ANOVA) of regression parameters of the predicted response surface quadratic model for diuron degradation percentage was shown in Table 4.14. It appeared that 3 parameters have impacted on the model, 3 i.e. B, C, and AB (P – value < 0.0100). These were pH

level, applied voltage and interaction of chloride ion and pH. These parameters were significant model terms.

Table 4.14 ANOVA for the RSM model for diuron degradation percentage.

Source	Degree of freedom (df)	Sum of square (SS)	Mean square	F – value	P – value
A	1	3.85	3.85	0.46	0.5262
B	1	1479.41	1479.41	178.11	< 0.0001
C	1	257.87	257.87.	31.05	0.0026
AB	1	162.18	162.18	19.52	0.0069
AC	1	9.12	9.12	1.10	0.3427
BC	1	16.48	16.48	1.98	0.2180
A^2	1	1.32	1.32	0.16	0.7062
B^2	1	4.40	4.40	0.53	0.4995
C^2	1	95.80	95.80	11.53	0.0193
Model	9	2030.58	225.62	27.16	0.0010
Error	5	41.53	8.31		
Total	14	2072.11			

จุฬาลงกรณ์มหาวิทยาลัย
Chulalongkorn University

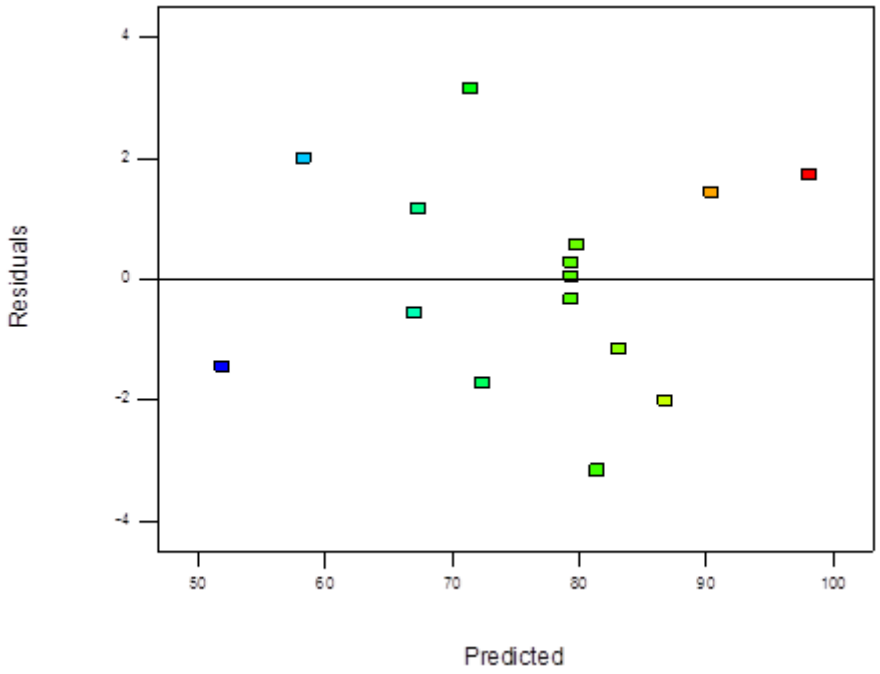

Figure 4.28 Residual plot of diuron degradation percentage.

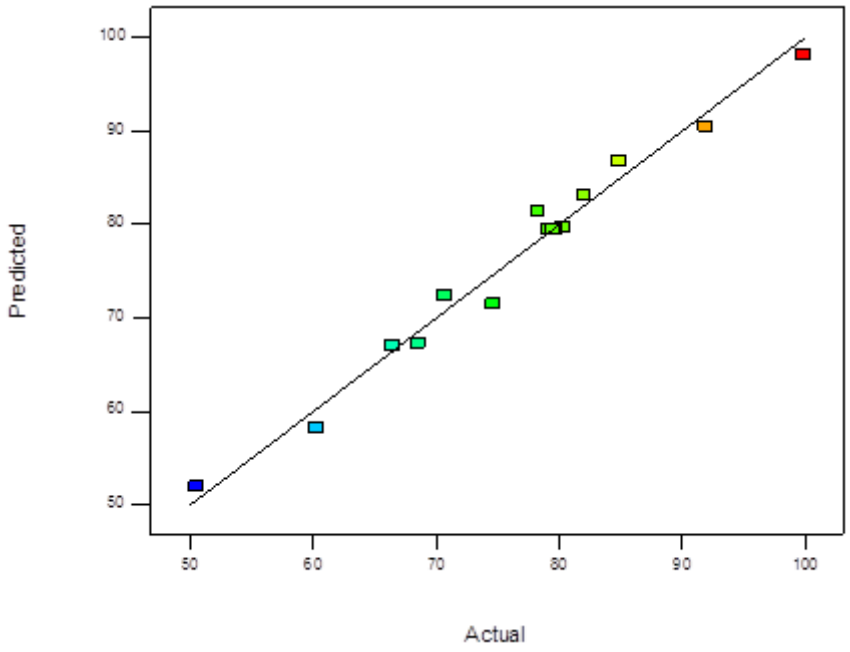

Figure 4.29 Comparison diuron degradation percentages between the predicted values and the actual values of RSM – BBD model.

From the residual plot (Figure 4.28) presented, overall data are well dispersed in negative and positive zone. Furthermore, R – squared or satisfactory coefficient of determination (Figure 4.29) is 0.9800. Both previous results confirmed that the RSM-BBD model could be used to predict diuron degradation performance.

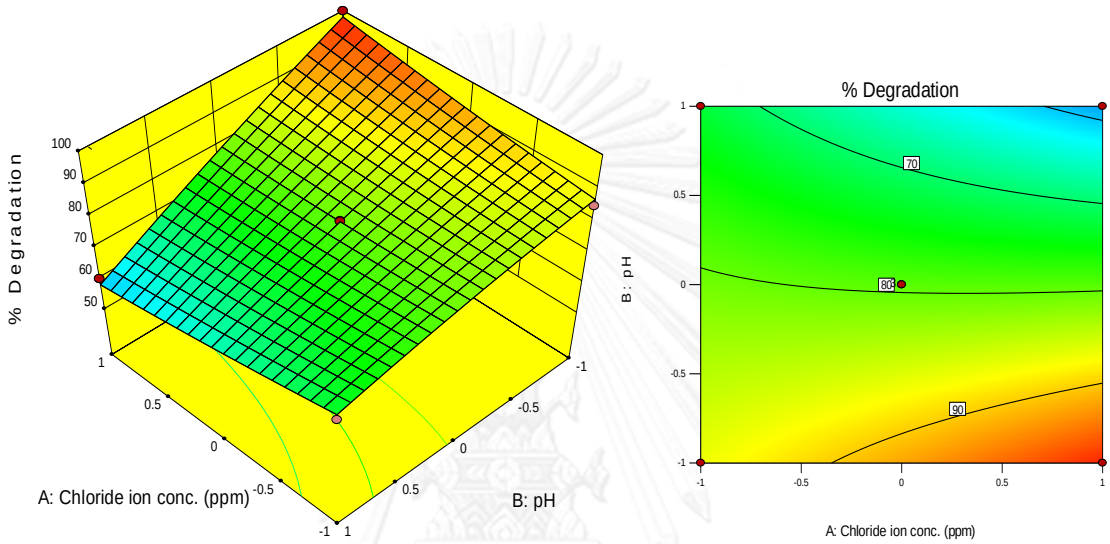

Figure 4.30 Chloride ion concentration and pH 3D surface and Chloride ion concentration and pH contour of predicted degradation percentage.

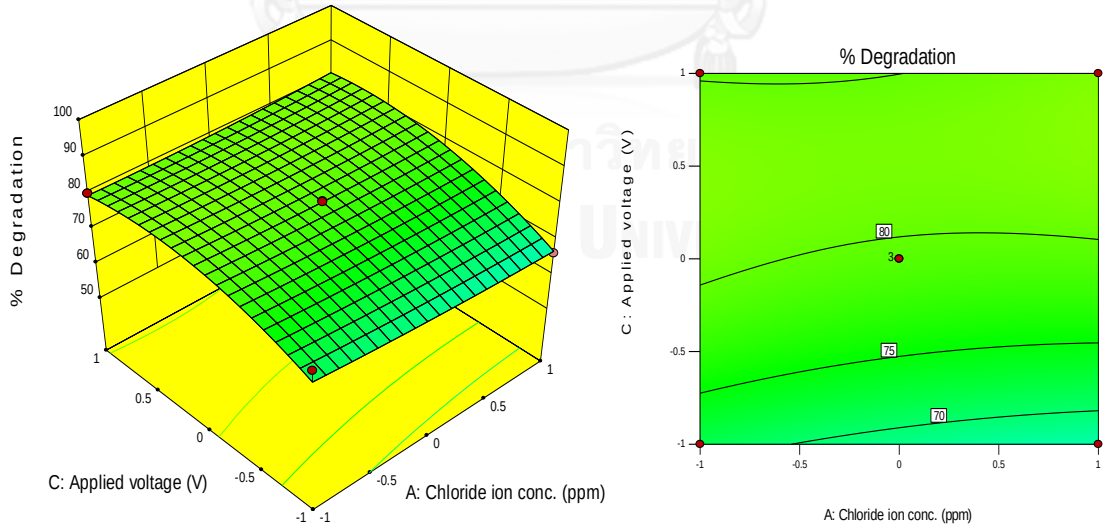

Figure 4.31 Chloride ion concentration and applied voltage 3D surface and Chloride ion concentration and applied voltage contour of predicted degradation percentage.

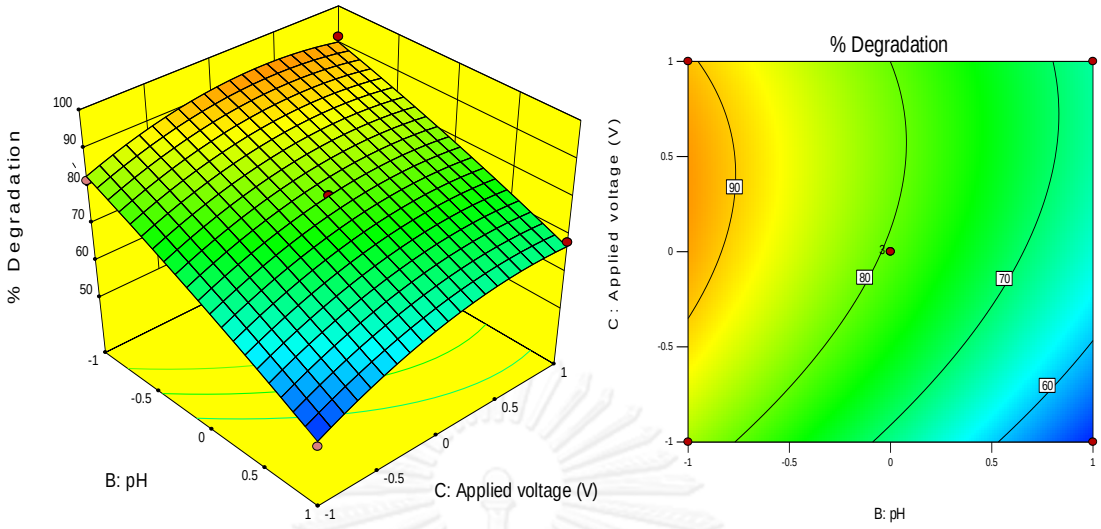

Figure 4.32 pH and applied voltage 3D surface and pH and applied voltage contour of predicted degradation percentage.

Figure 4.30 – 4.32 show trend of diuron degradation. Chloride ion was added to the solution. It was increasing conductivity so electron was easily transferred. However, concentration of chloride ion has impact on diuron degradation when pH was changed. At the increase of chloride ion and decrease of pH, diuron was degraded effectively compared with the decrease of chloride ion and increase of pH. The result showed the relation between chloride ion and pH that affected performance of diuron degradation, but, the applied voltage had no effect together with chloride ion. This result was confirmed by 2^k factorial design that shown in previous section. This result was shown in Figure 4.30 – 4.31. Figure 4.32 gave a result the same previous topic. Diuron was rapidly degraded when bias potential is increased and pH value is dropped. The pH level was significant for diuron degradation.

When the mathematical model was used to predict diuron degradation, from Figure 4.33, diuron degradation is better while in acidic condition (pH<7). The result shows that the increase of chloride ion leading to better diuron degradation. In nature pH, increase of chloride ion would not significantly affect to diuron degradation resulting in the constant diuron degradation. On the other hand, in alkaline condition, increase of chloride ion yields the decrease of diuron degradation. Figure 4.34 shows that pH and applied voltage has synergistic effect. When pH is

decreased and applied voltage is increased, diuron degradation is also increased. The effect of pH and applied voltage are discussed in section 4.4. From Figure 4.35, when the applied voltage is increased and chloride ion is decrease, diuron degradation is increased to the maximum value after that the efficiency of diuron degradation is decreased.

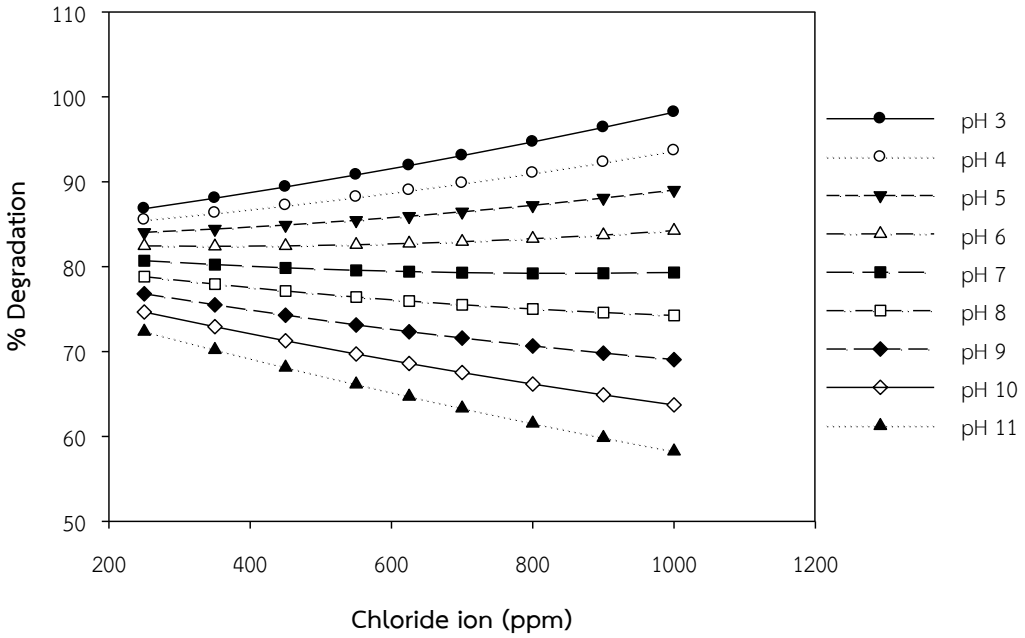

Figure 4.33 Predicted degradation percentages via the mathematical model under applied voltage 2.5 V.

จุฬาลงกรณ์มหาวิทยาลัย
Chulalongkorn University

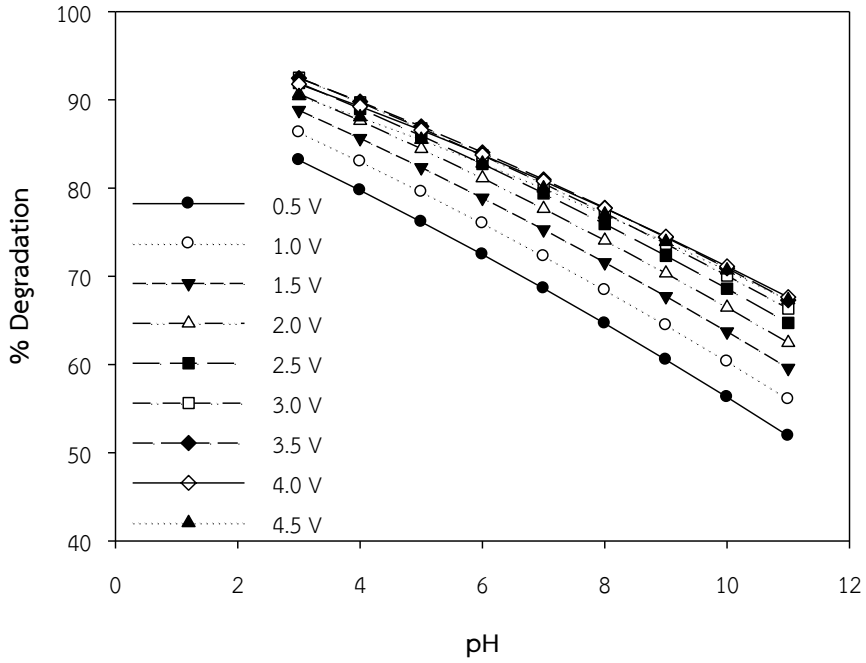

Figure 4.34 Predicted degradation percentages via the mathematical model under concentration of chloride ion 625 ppm.

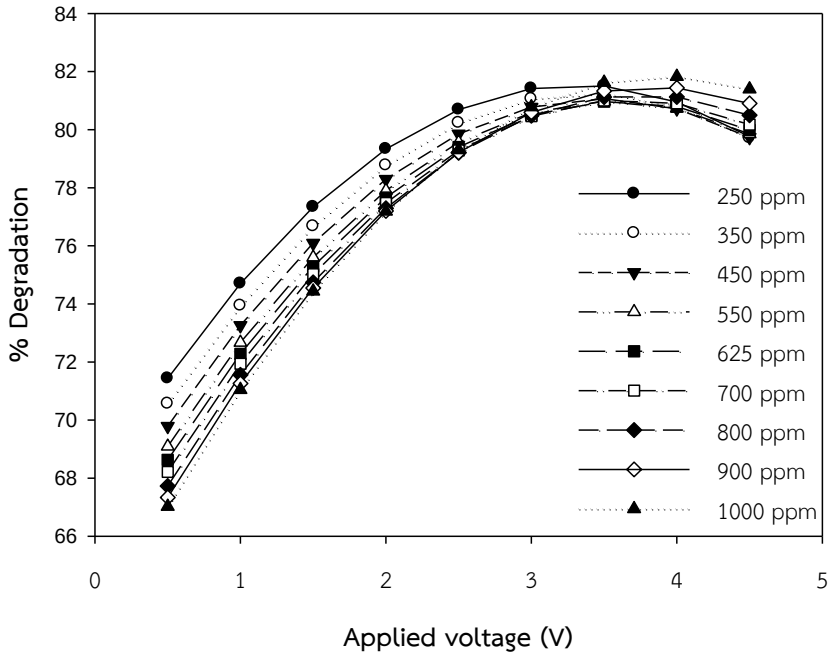

Figure 4.35 Predicted degradation percentages via the mathematical model under pH 7.

Moreover, the apparent rate constant was predicted by RSM – BBD. It analyzed apparent rate constant derived from data obtained from the first 120 minutes. The pseudo – first order equation was used.

The mathematical model was used for reply to apparent rate constant at 120 minute:

$$\hat{y} = 5.433 \times 10^{-3} + 1.463A \times 10^{-3} - 3.600B \times 10^{-3} + 8.125C \times 10^{-4}$$
$$- 2.950AB \times 10^{-3} + 6.750AC \times 10^{-4} + 3.000BC \times 10^{-4}$$
$$+ 1.246A^2 \times 10^{-3} + 1.521B^2 \times 10^{-3} - 1.454C^2 \times 10^{-3}$$

The analysis of variance (ANOVA) of regression parameters of the predicted response surface quadratic model for the apparent rate constant at 120 minute was shown in Table 4.15. It appeared that 1 parameter has impacted to model. It was pH level that was significant model terms because of P – value < 0.0100. Figure 4.36 shown residual plot of the apparent rate constant at 120 minute. Dispersion of data was almost equaled but R – squared was calculated in Figure 4.37. It was 0.8465. As the result, the experimental results could not be described with the model. So, the rate constant of degradation was difficult to predict by statistical method.

จุฬาลงกรณ์มหาวิทยาลัย
Chulalongkorn University

Table 4.15 ANOVA for the RSM model for k_{app} at 120 minute.

Source	Degree of freedom (df)	Sum of square (SS)	Mean square	F – value	P – value
A	1	1.711×10^{-5}	1.711×10^{-5}	2.53	0.1726
B	1	1.037×10^{-4}	1.037×10^{-4}	15.32	0.0112
C	1	5.281×10^{-6}	5.281×10^{-6}.	0.78	0.4174
AB	1	3.481×10^{-5}	3.481×10^{-5}	5.14	0.0726
AC	1	1.823×10^{-6}	1.823×10^{-6}	0.27	0.6259
BC	1	3.600×10^{-7}	3.600×10^{-7}	0.053	0.8267
A^2	1	5.731×10^{-6}	5.731×10^{-6}	0.85	0.3996
B^2	1	8.540×10^{-6}	8.540×10^{-6}	1.26	0.4995
C^2	1	7.808×10^{-6}	7.808×10^{-6}	1.15	0.3318
Model	9	1.865×10^{-4}	2.072×10^{-5}	3.06	0.1152
Error	5	3.383×10^{-5}	6.766×10^{-6}		
Total	14	2.204×10^{-4}			

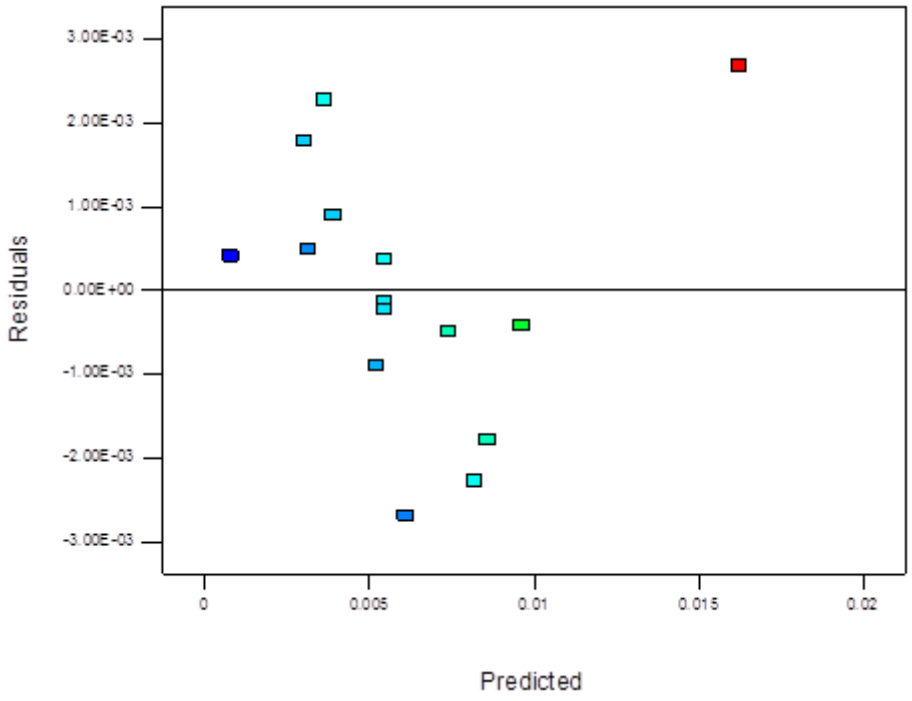

Figure 4.36 Residual plot of the apparent rate constant at 120 minute.

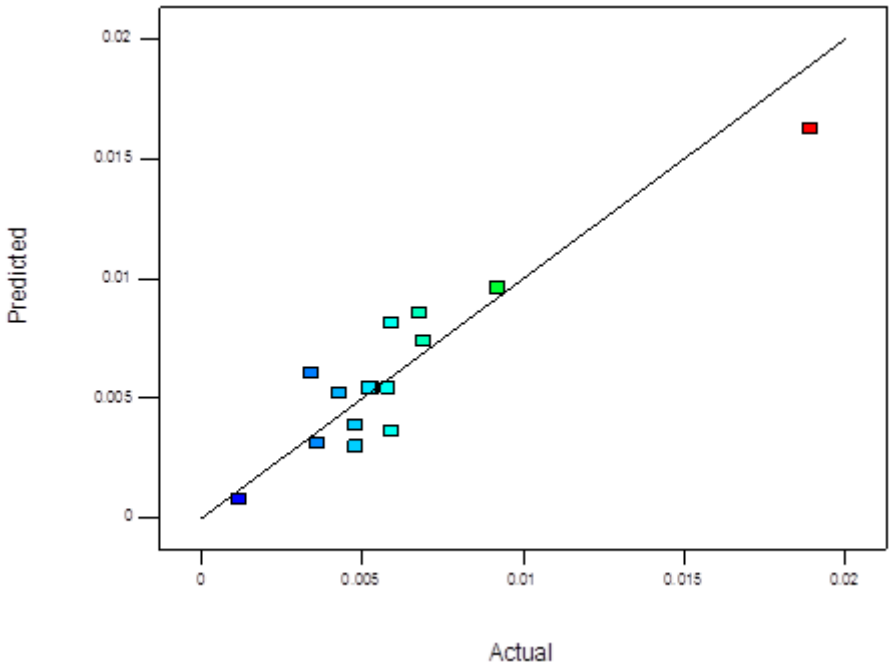

Figure 4.37 Comparison the apparent rate constant at 120 minute between the predicted values and the actual values of RSM – BBD model.

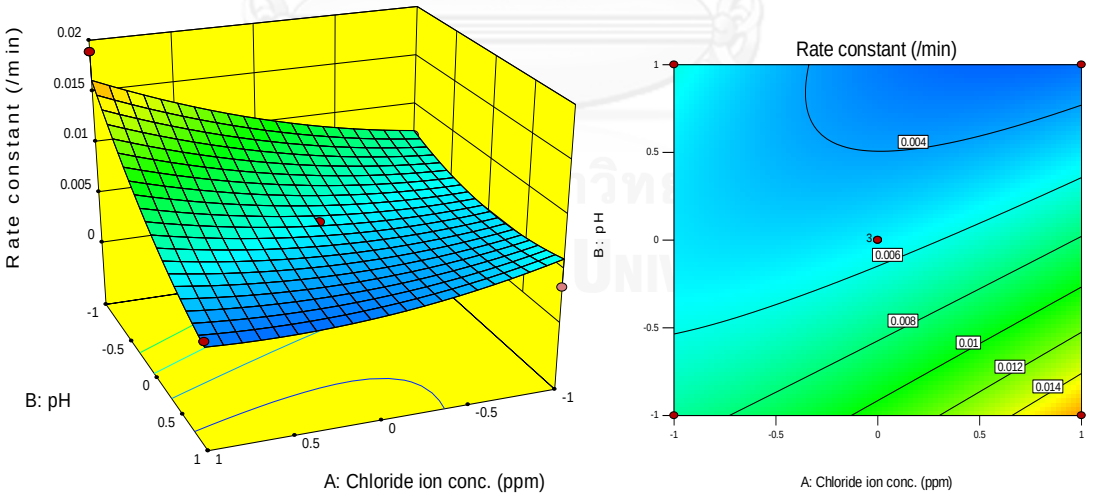

Figure 4.38 Chloride ion concentration and pH 3D surface and Chloride ion concentration and pH contour of predicted the apparent rate constant at 120 minute.

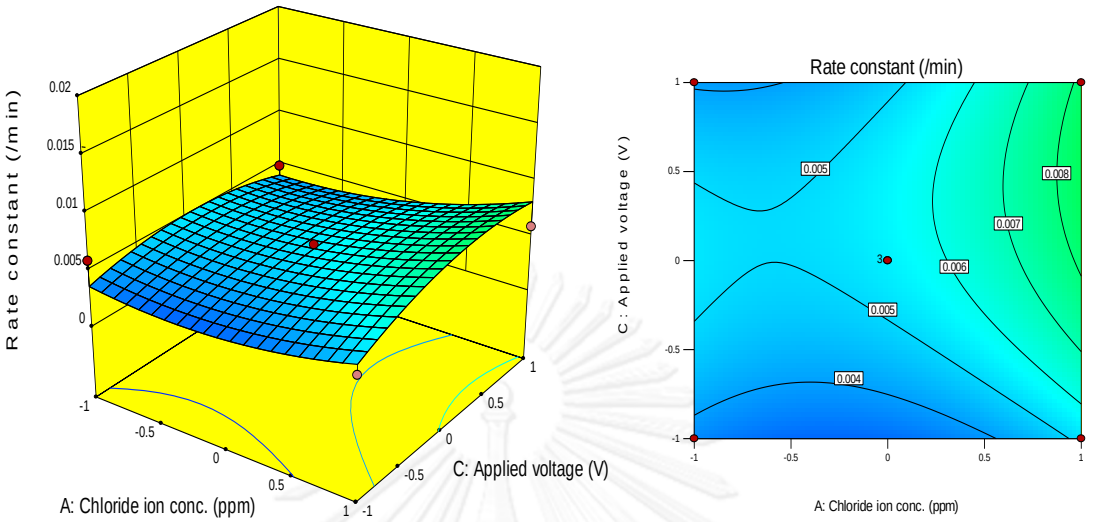

Figure 4.39 Chloride ion concentration and applied voltage 3D surface and Chloride ion concentration and applied voltage contour of predicted the apparent rate constant at 120 minute.

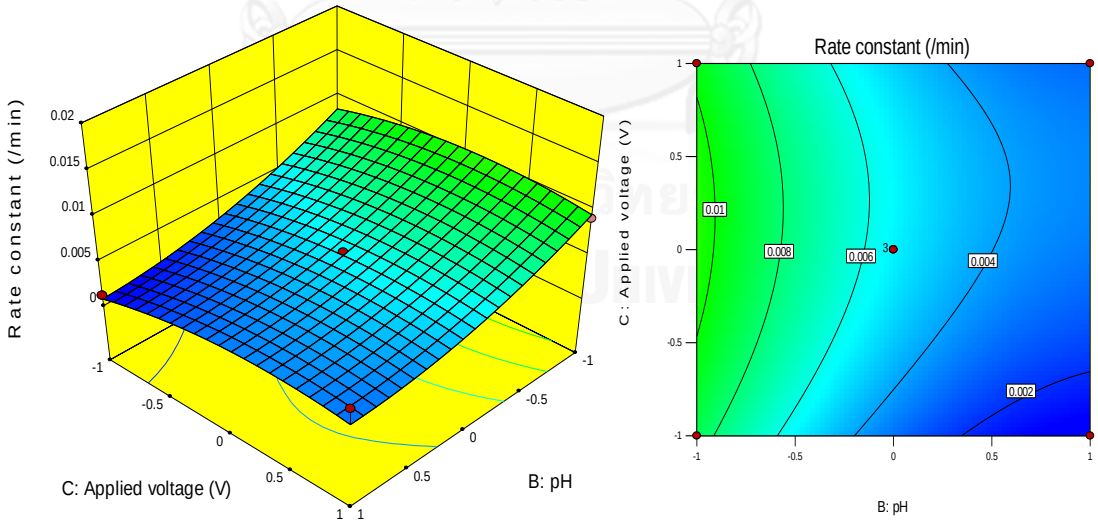

Figure 4.40 pH and applied voltage 3D surface and pH and applied voltage contour of predicted the apparent rate constant at 120 minute.

The apparent rate constant was increased when pH level was decreased and high chloride ion concentration. It was presented in Figure 4.38. In contrast, interaction effect of applied voltage both chloride ion concentration and pH level were hardly impact to the apparent rate constant. They was shown in Figure 4.39 – 4.40. Relation between pH level and applied voltage was a little effect.

When the mathematical model was used to predict the apparent rate constant at 120 minute, illustrated in Figure 4.41, the apparent rate constant is increased when chloride ion is increased and pH is decreased. However, at pH 11, the apparent rate constant is decreased when chloride ion is increased. From Figure 4.42, when pH is decreased and applied voltage is increased, the apparent rate constant is increased. The result indicates that when the applied voltage and chloride ion are both increased, the apparent rate constant is increased to the maximum value then the apparent rate constant tends to drop as shown in Figure 4.43.

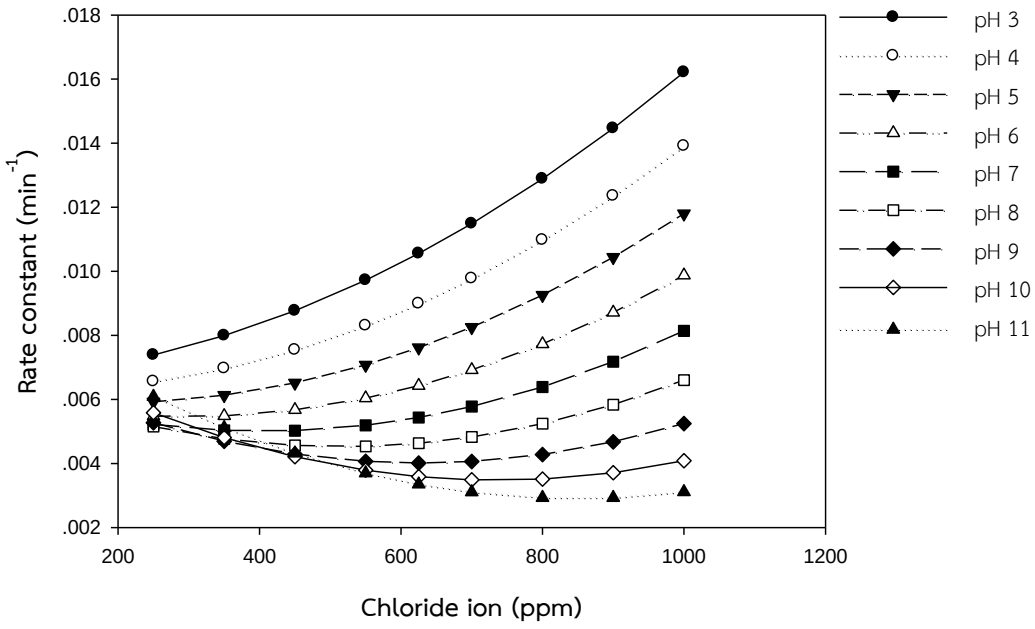

Figure 4.41 Predicted the apparent rate constant at 120 minute via the mathematical model under applied voltage 0.5 V.

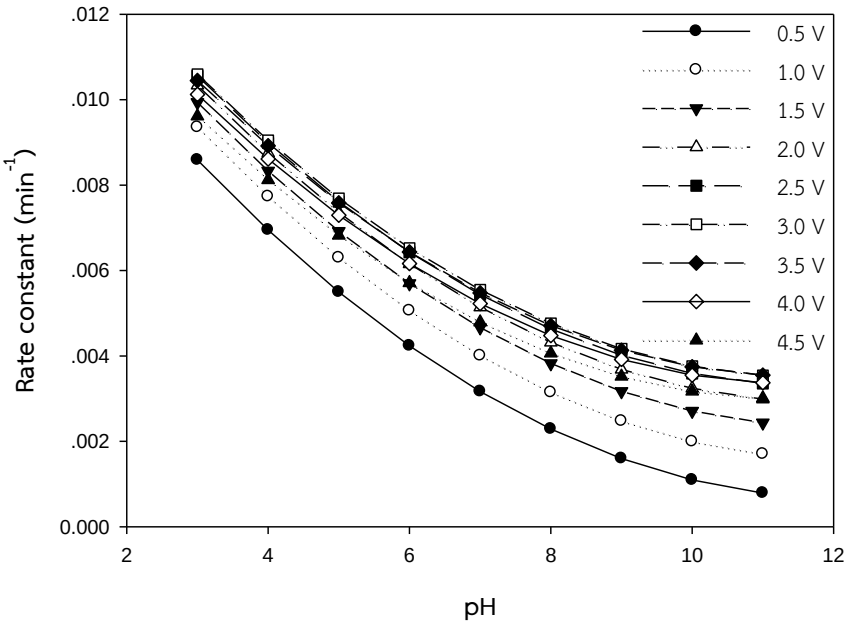

Figure 4.42 Predicted the apparent rate constant at 120 minute via the mathematical model under concentration of chloride ion 625 ppm.

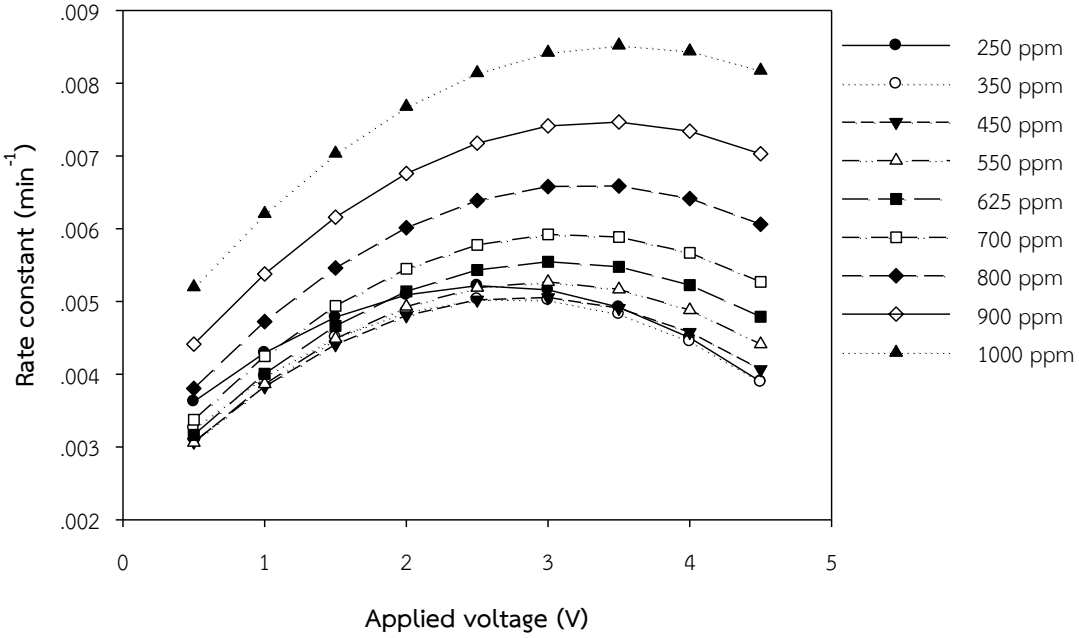

Figure 4.43 Predicted the apparent rate constant at 120 minute via the mathematical model under pH 7.

However, rate constant at after 120 minutes of degradation was not reported because the pseudo-first order model could not be used to determine the rate constant. After 120 minutes, diuron concentration was not only the parameter that expresses the rate of reaction, the concentration of intermediate formed during the degradation should be taken into account. This reason has been discussed before in the previous section.

จุฬาลงกรณ์มหาวิทยาลัย
Chulalongkorn University

CHAPTER V
CONCLUSION

5.1 Summary of the results

i. Photoelectrocatalysis can be used to effectively degrade diuron.

ii. Both pH and applied voltage have high impact on degradation of diuron.

5.2 Conclusions

Diuron can be degraded by photoelectrocatalysis. Titanium substrate coated with titania was used as anode while graphite was used as cathode. Various parameters were analyzed via RSM – BBD. Efficiency of diuron degradation depended on effect of pH, applied voltage and chloride ion. Whereas, the apparent rate constant at 120 minute depended on pH and applied voltage. For the apparent rate constant at 420 minute, it was difficult to predict because the apparent rate constant depended on one of intermediates instead of diuron.

5.3 Recommendations for future work

i. Identification of intermediates of diuron by using LC – MS/MS.

ii. Separation and analysis anion in solution.

iii. Change system to continuous process.

จุฬาลงกรณ์มหาวิทยาลัย
Chulalongkorn University

REFERENCES

[1] Giacomazzi, S. and Cochet, N. Environmental impact of diuron transformation: a review. Chemosphere 56 (2004): 1021-1032.

[2] Katsumata, H., Sada, M., Nakaoka, Y., Kaneco, S., Suzuki, T., and Ohta, K. Photocatalytic degradation of diuron in aqueous solution by platinized TiO2. Journal of Hazardous Materials 171 (2009): 1081-1087.

[3] Katal, R., Baei, M.S., Rahmati, H.T., and Esfandian, H. Kinetic, isotherm and thermodynamic study of nitrate adsorption from aqueous solution using modified rice husk. Journal of Industrial and Engineering Chemistry 18 295-302.

[4] Salvestrini, S., Di Cerbo, P., and Capasso, S. Kinetics of the chemical degradation of diuron. Chemosphere 48 (2002): 69-73.

[5] Akcha, F., Spagnol, C., and Rouxel, J. Genotoxicity of diuron and glyphosate in oyster spermatozoa and embryos. Aquatic Toxicology 106-107 (2012) 104-113.

[6] Fujishima, A., Rao, T.N., and Tryk, D.A. Titanium dioxide photocatalysis. Journal of Photochemistry and Photobiology C: Photochemistry Reviews 1 (2000): 1-21.

[7] Al-Degs, Y.S., El-Sheikh, A.H., and Jaber, S.T. Application of heated date seeds as a novel extractant for diuron from water. Arabian Journal of Chemistry 6 121-129.

[8] Dayan, F.E. and Zaccaro, M.L.d.M. Chlorophyll fluorescence as a marker for herbicide mechanisms of action. Pesticide Biochemistry and Physiology 102 189-197.

[9] Sharma, P. and Suri, C.R. Biotransformation and biomonitoring of phenylurea herbicide diuron. Bioresource Technology 102 3119-3125.

[10] Omar Bouras, J.-C.B., Michel Baudu, Hussein Khalaf Adsorption of diuron and its degradation products from aqueous solution by surfactant-modified pillared clays. Applied Clay Science 37 (2007): 240-250.

[11] Djebbar, K.E., Zertal, A., Debbache, N., and Sehili, T. Comparison of Diuron degradation by direct UV photolysis and advanced oxidation processes. Journal of Environmental Management 88 (2008): 1505-1512.

[12] Oturan, M.A., Edelahi, M.C., Oturan, N., El kacemi, K., and Aaron, J.-J. Kinetics of oxidative degradation/mineralization pathways of the phenylurea herbicides diuron, monuron and fenuron in water during application of the electro-Fenton process. Applied Catalysis B: Environmental 97 82-89.

[13] Oturan, N., Trajkovska, S., Oturan, M.A., Couderchet, M., and Aaron, J.-J. Study of the toxicity of diuron and its metabolites formed in aqueous medium during application of the electrochemical advanced oxidation process electro-Fenton. Chemosphere 73 (2008): 1550-1556.

[14] R. Daghrira, P. Droguia, and Robert, D. Photoelectrocatalytic technologies for environmental applications. Journal of Photochemistry and Photobiology A: Chemistry 238 (2012): 41-52.

[15] Hyunwoong Park, Y.P., Wooyul Kim, Wonyong Choi Surface modification of TiO_2 photocatalyst for environmental applications. Journal of Photochemistry and Photobiology C: Photochemistry Reviews 15 (2013): 1-20.

[16] Yerokhin, A.L., Nie, X., Leyland, A., Matthews, A., and Dowey, S.J. Plasma electrolysis for surface engineering. Surface and Coatings Technology 122 (1999): 73-93.

[17] Selcuk, H. and Bekbolet, M. Photocatalytic and photoelectrocatalytic humic acid removal and selectivity of TiO_2 coated photoanode. Chemosphere 73 (2008): 854-858.

[18] Selcuk, H., Sene, J.J., and Anderson, M.A. Photoelectrocatalytic humic acid degradation kinetics and effect of pH, applied potential and inorganic ions. Journal of Chemical Technology & Biotechnology 78 (2003): 979-984.

[19] Xiaoli, Y., Huixiang, S., and Dahui, W. Photoelectrocatalytic degradation of phenol using a TiO_2/Ni thin-film electrode. Korean Journal of Chemical Engineering 20 (2003): 679-684.

[20] Cardoso, J.C., Lizier, T.M., and Zanoni, M.V.B. Highly ordered TiO2 nanotube arrays and photoelectrocatalytic oxidation of aromatic amine. Applied Catalysis B: Environmental 99 96-102.

[21] Viswanathan, K.R.J.A.a.B. Effect of surface area, pore volume and particle size of P25 titania on the phase transformation of anatase to rutile. Indian Journal of Chemistry 48A (2009): 1378-1382.

[22] Nelieu, S., Shankar, M.V., Kerhoas, L., and Einhorn, J. Phototransformation of monuron induced by nitrate and nitrite ions in water: Contribution of photonitration. Journal of Photochemistry and Photobiology A: Chemistry 193 (2008): 1-9.

[23] Shankar, M.V., Nelieu, S., Kerhoas, L., and Einhorn, J. Natural sunlight NO_3^-/NO_2^--induced photo-degradation of phenylurea herbicides in water. Chemosphere 71 (2008): 1461-1468.

[24] Bosko, M.L., Rodrigues, M.A.S., Ferreira, J.Z., Miro, E.E., and Bernardes, A.M. Nitrate reduction of brines from water desalination plants by membrane electrolysis. Journal of Membrane Science 451 276-284.

[25] Polatides, C., Dortsiou, M., and Kyriacou, G. Electrochemical removal of nitrate ion from aqueous solution by pulsing potential electrolysis. Electrochimica Acta 50 (2005): 5237-5241.

[26] Zeng, X., Gan, Y.X., Clark, E., and Su, L. Amphiphilic and photocatalytic behaviors of TiO_2 nanotube arrays on Ti prepared via electrochemical oxidation. Journal of Alloys and Compounds 509 L221-L227.

[27] Linsebigler, A.L., Lu, G., and Yates, J.T. Photocatalysis on TiO_2 Surfaces: Principles, Mechanisms, and Selected Results. Chemical Reviews 95 (1995): 735-758.

[28] Seferlis, A.K. and Neophytides, S.G. On the kinetics of photoelectrocatalytic water splitting on nanocrystalline TiO_2 films. Applied Catalysis B: Environmental 132-133 543-552.

[29] Zhang, Y., Xiong, X., Han, Y., Zhang, X., Shen, F., Deng, S., Xiao, H., Yang, X., Yang, G., and Peng, H. Photoelectrocatalytic degradation of recalcitrant organic pollutants using TiO2 film electrodes: An overview. Chemosphere 88 145-154.

[30] Hzcan, L., Yurdakal, S., Augugliaro, V., Loddo, V., Palmas, S., Palmisano, G., and Palmisano, L. Photoelectrocatalytic selective oxidation of 4-methoxybenzyl alcohol in water by TiO_2 supported on titanium anodes. Applied Catalysis B: Environmental 132-133 535-542.

[31] Li, X.Z., Li, F.B., Fan, C.M., and Sun, Y.P. Photoelectrocatalytic degradation of humic acid in aqueous solution using a Ti/TiO_2 mesh photoelectrode. Water Research 36 (2002): 2215-2224.

[32] Li, X.Z., Liu, H.L., Yue, P.T., and Sun, Y.P. Photoelectrocatalytic Oxidation of Rose Bengal in Aqueous Solution Using a Ti/TiO_2 Mesh Electrode. Environmental Science & Technology 34 (2000): 4401-4406.

[33] Kamat, P.V. Photophysical, Photochemical and Photocatalytic Aspects of Metal Nanoparticles. The Journal of Physical Chemistry B 106 (2002): 7729-7744.

[34] Neumann-Spallart, M. Aspects of Photocatalysis on Semiconductors: Photoelectrocatalysis. TRANSFORMATION AND STORAGE OF SOLAR ENERGY 61 (2007): 806-809.

[35] Li J., L.L., Zheng L., Xian Y., Jin L. Photoelectrocatalytic degradation of rhodamine B using Ti/TiO_2 electrode prepared by laser calcination method. Electrochim. Acta , 51 (2006): 4942-4949.

[36] Wang N., L.X., Wang Y., Quan X., Chen G. Evaluation of bias potential enhanced photocatalytic degradation of 4-chlorophenol with TiO_2 nanotube fabricated by anodic oxidation method. Chemical Engineering Journal 146 (2009a): 30 - 35.

Chulalongkorn University

APPENDICES

จุฬาลงกรณ์มหาวิทยาลัย
Chulalongkorn University

APPENDIX A CALIBRATION CURVE OF DIURON

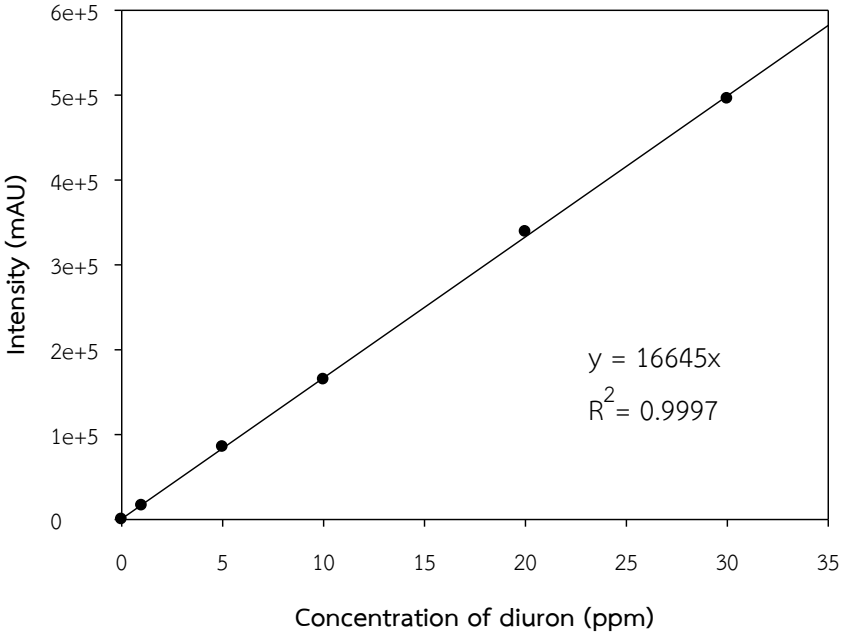

Figure A1 Calibration curve of diuron.

จุฬาลงกรณ์มหาวิทยาลัย
Chulalongkorn University

APPENDIX B CALIBRATION CURVE OF NITRATE

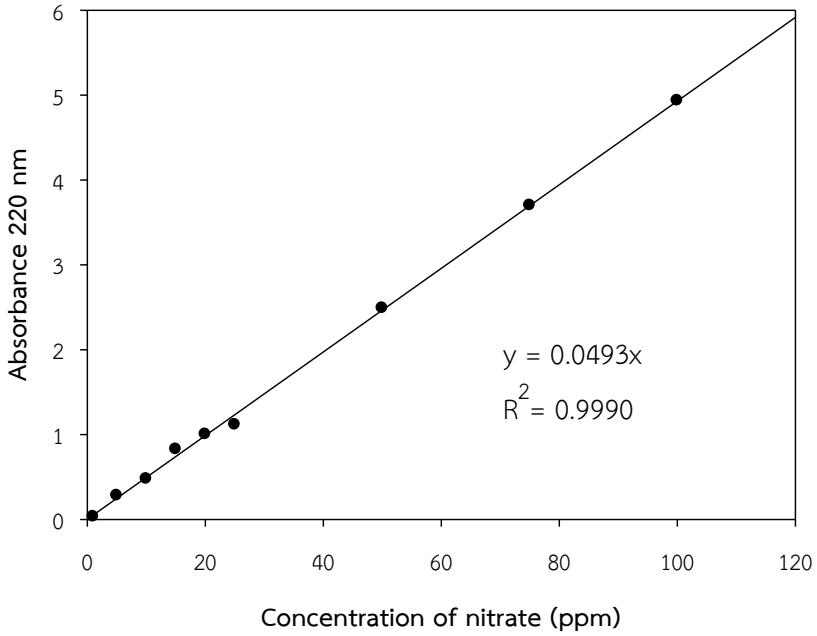

Figure B1 Calibration curve of nitrate.

จุฬาลงกรณ์มหาวิทยาลัย
Chulalongkorn University

APPENDIX C CALIBRATION CURVE OF NITRITE

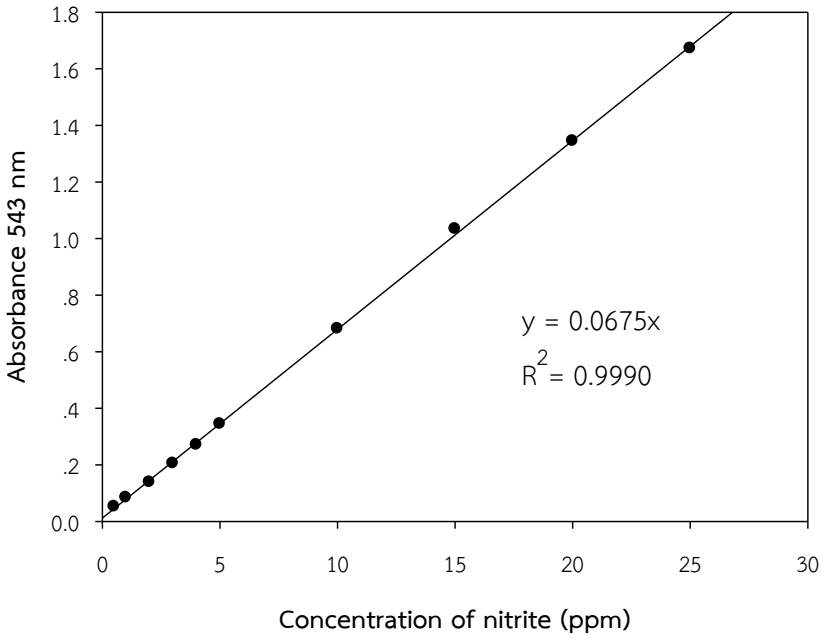

Figure C1 Calibration curve of nitrite.

จุฬาลงกรณ์มหาวิทยาลัย
Chulalongkorn University

APPENDIX D CALCULATION OF THE CRYSTALLITE SIZE

The crystallite size was calculated using the Debye – Scherrer equation.

$$D = \frac{k\lambda}{\beta \cos\theta}$$

where D = Crystallite size, Å

k = Crystallite-shape factor = 0.9

λ = X-ray wavelength, 1.5406 Å for Cu$K\alpha$

θ = Observed peak angle, degree

β = X – ray diffraction broadening

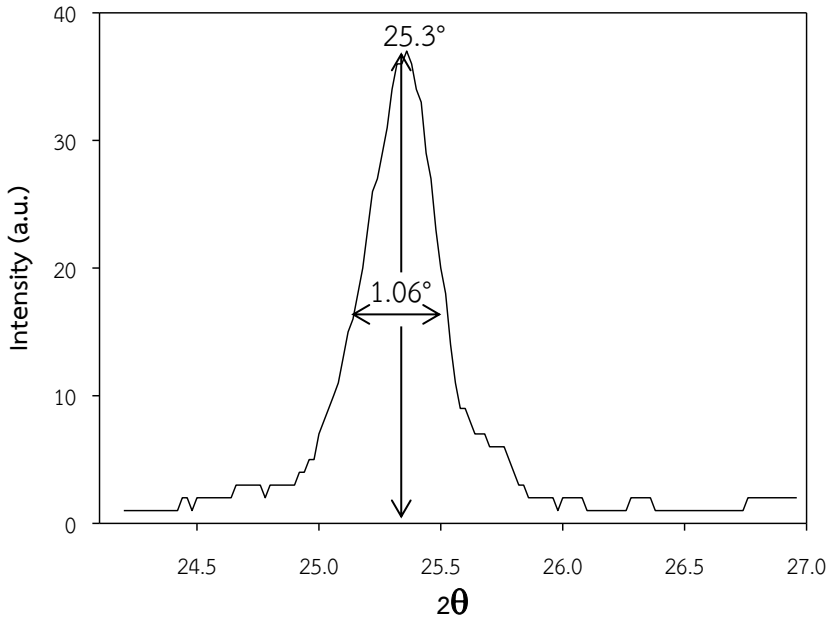

Figure D1 The observation peak of anatase phase for calculating the crystallite size.

Example: Calculation of the crystallite size of anatase phase

The half – height width of anatase phase diffraction peak (β)

β = 1.06° (from Figure D1)

β = (2π x 1.06°)/360

β = 0.0185 radian

and 2θ = 25.3°

θ = 12.65°

Thus, the crystallite size = $\frac{0.9 \times 1.5406}{0.0185\cos 12.65}$

D = 76.81 nm

จุฬาลงกรณ์มหาวิทยาลัย
Chulalongkorn University

APPENDIX E CALCULATION OF PHASE COMPOSITION OF TITANIA

Phase component was determined from relation of peak intensity of anatase (I_A) and rutile (I_R) [21].

$$\text{Anatase} = \frac{0.79I_A}{0.79I_A + I_R}$$

$$\text{Rutile} = \frac{I_R}{0.79I_A + I_R}$$

Where I_A is a peak intensity of anatase phase at 25.3° and I_R is a peak intensity of rutile phase at 27.4°.

Example: Calculation of phase composition of anatase phase

Peak intensity of anatase and rutile shows in Figure E1 and E2, respectively.

Thus, $$\text{Anatase} = \frac{0.79 \times 37.0}{(0.79 \times 37.0) + 7}$$

$$\text{Anatase} = 78.05\%$$

จุฬาลงกรณ์มหาวิทยาลัย
Chulalongkorn University

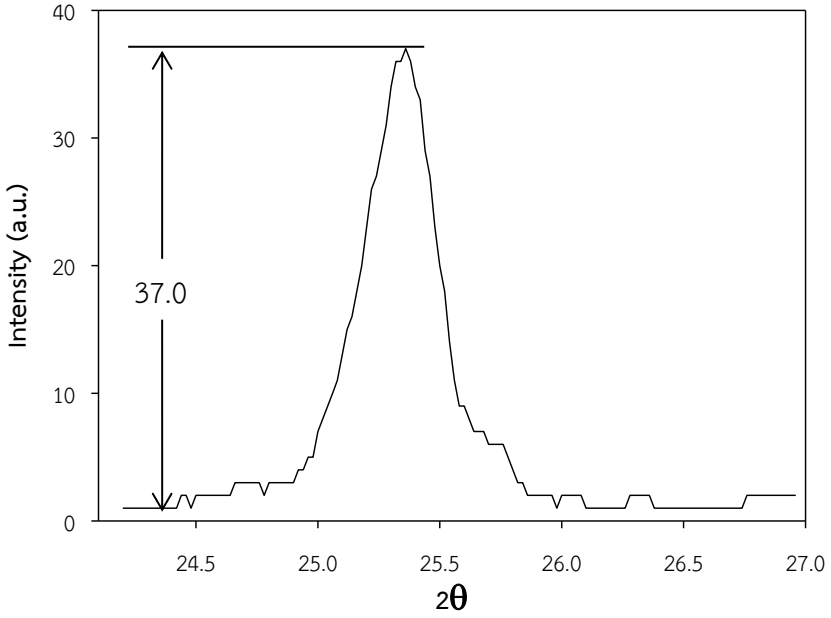

Figure E1 The observation peak of anatase phase for calculating phase composition.

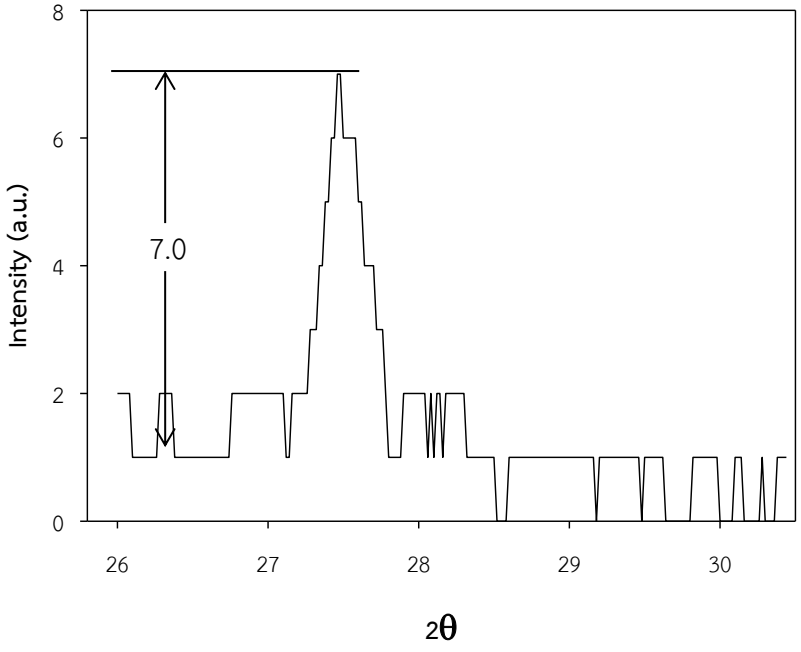

Figure E2 The observation peak of rutile phase for calculating phase composition.

APPENDIX F CODING DATA

Coding data change data, which it is qualitatively or quantitatively data. Coded data is analyzed easy via statistical technique. Data is normalized via below equation.

$$X_{coded} = \frac{\text{Data in interested range} - \text{Average of sum between high and low value}}{\text{Average of difference between high and low value}}$$

$$\mathbf{X_{coded}} = \frac{X_{uncoded} - \frac{X_{uncoded,\,highest} + X_{uncoded,\,lowest}}{2}}{\frac{X_{uncoded,\,highest} - X_{uncoded,\,lowest}}{2}}$$

Example: Calculation of coding data (pH)

In this study, pH interested in range 3 – 11.

$$X_{coded} = \frac{X_{uncoded} - \frac{3 + 11}{2}}{\frac{3 - 11}{2}}$$

$$X_{coded} = \frac{x - 7}{4}$$

จุฬาลงกรณ์มหาวิทยาลัย
Chulalongkorn University

APPENDIX G CALCULATION OF MAIN AND INTERACTION EFFECT

Main and interaction effects were determined by these equations.

β_0 = average of all responses (y_i)

The main effect = average value of responses from all runs at the high level of the factor – average value of responses from all runs at the low level of the factor

The interaction effect = average value of one factor on responses from all runs on the high level of another factor – average value of one factor responses from all runs on the low level of another factor

Example:

Table G1 The level of the factor.

Run	X_1	X_2	X_3	X_1X_2	X_1X_3	X_2X_3	$X_1X_2X_3$	y_i
1	-1	-1	-1	1	1	1	-1	81.22
2	1	-1	-1	-1	-1	1	1	99.71
3	-1	1	-1	-1	1	-1	1	35.85
4	1	1	-1	1	-1	-1	-1	57.04
5	-1	-1	1	1	-1	-1	1	100.00
6	1	-1	1	-1	1	-1	-1	74.13
7	-1	1	1	-1	-1	1	-1	24.99
8	1	1	1	1	1	1	1	68.61

จุฬาลงกรณ์มหาวิทยาลัย
Chulalongkorn University

$$\beta_0 = \frac{81.22 + 99.71 + 35.85 + 57.04 + 100.00 + 74.13 + 24.99 + 68.61}{8}$$

β_0 = 67.69

$$\beta_1 = \frac{[(1)(99.71 + 57.04 + 74.13 + 68.61)]}{4} + \frac{[(-1)(81.22 + 35.85 + 100.00 + 24.99)]}{4}$$

β_1 = 14.36

$$\beta_{12} = \frac{[(1)(81.22 + 57.04 + 100.00 + 68.61)]}{4} + \frac{[(-1)(99.71 + 35.85 + 74.13 + 24.99)]}{4}$$

$$\beta_{12} = 18.05$$

จุฬาลงกรณ์มหาวิทยาลัย
Chulalongkorn University

APPENDIX H NORMAL PROBABILITY PLOT

There are several 5 steps.

i. To rearrange parameter values from high to low value.

ii. To add order of parameter values

iii. To calculate cumulative probability (P_i)

$$P_i = \frac{(i - 0.5)}{n}$$

Where i = rake of each effect

n = number of effect

iv. To make table of P_i (Table H1)

v. To plot P_i and calculated effect (Figure H1)

Table H1 Cumulative probability.

Rank(i)	Value	Effect	P_i	P_i x 100
1	-42.14	X_2	0.0714	7.14
2	-5.48	X_1X_3	0.2143	21.43
3	1.52	X_3	0.3571	35.71
4	1.88	X_2X_3	0.5000	50.00
5	14.36	X_1	0.6429	64.29
6	16.70	$X_1X_2X_3$	0.7857	78.57
7	18.05	X_1X_2	0.9285	92.86

จุฬาลงกรณ์มหาวิทยาลัย
Chulalongkorn University

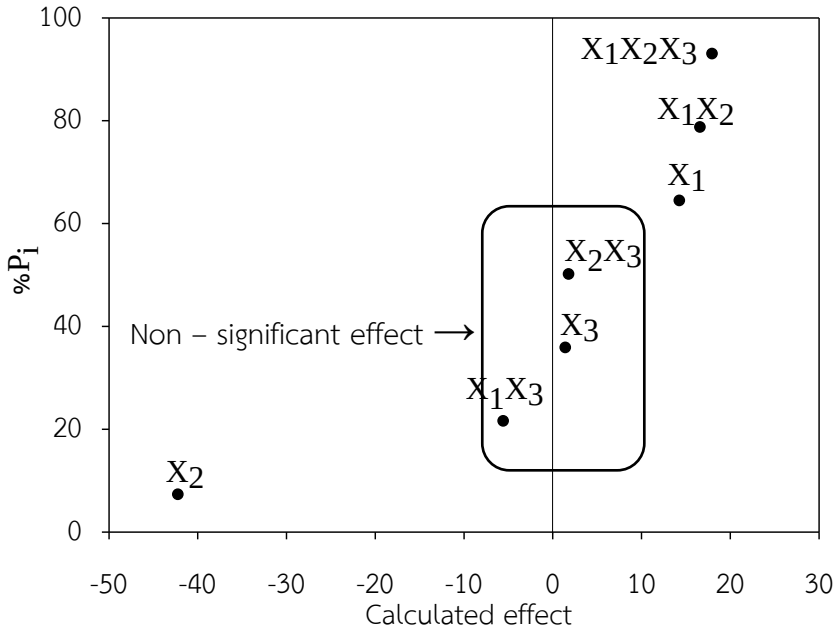

Figure H1 Cumulative probability plot.

จุฬาลงกรณ์มหาวิทยาลัย
Chulalongkorn University

APPENDIX I PRECISION OF CALCULATED EFFECT

There are several 5 steps.

i. To determine $S^2_{inherent}$

$$S^2_{inherent} = \frac{\sum(\text{value of non} - \text{significant effect})^2}{\text{Number of non} - \text{significant effect}}$$

$$S^2_{inherent} = \frac{(1.52)^2 + (-5.48)^2 + (1.88)^2}{3}$$

$$S^2_{inherent} = 11.97$$

ii. To determine standard deviation (S.D.)

$$S.D.^2 = \frac{4S^2_{inherent}}{2^k}$$, where k is number of factor

$$S.D. = 2.44$$

iii. To define t – distribution from t table

$$t_{(0.025,3)} = 3.182$$

iv. To determine confidence interval of calculated effect

Calculated effect ± $(t_{(0.025,3)})$(S.D.)

Calculated effect ± (3.182)(2.44)

Calculated effect ± 7.78

จุฬาลงกรณ์มหาวิทยาลัย
Chulalongkorn University

Table I1 Confidence interval of calculated effect.

Effect	Calculated effect	Lower limit	Upper limit
X_1	14.36	6.57	22.14
X_2	-42.14	-49.92	-34.35
X_3	1.52	-6.26	9.31
X_1X_2	18.05	10.26	25.83
X_1X_3	-5.48	-13.27	2.30
X_2X_3	1.88	-5.91	9.66
$X_1X_2X_3$	16.70	8.91	24.48

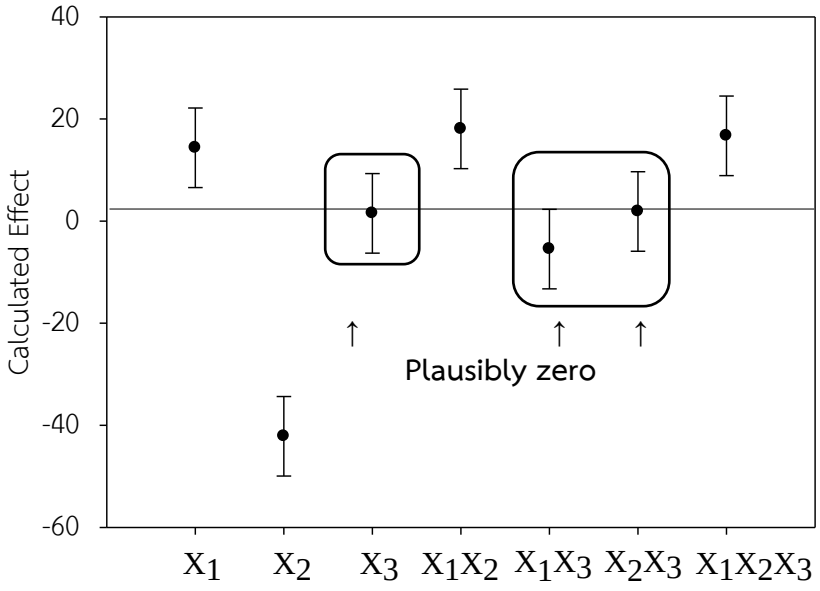

Figure I1 Confidence interval of calculated effect plot.

Chulalongkorn University

APPENDIX J ANOVA TABLE

There are several 3 steps.

i. To make ANOVA table

Table J1 The equation of ANOVA.

Source of variation	Degree of freedom (d.o.f.)	Sum of squares	Mean square	F – value
Regression	n – p	Sun of square error (SSR) = $\sum(\hat{y} - \bar{y})^2$	Mean square regression (MSR) = SSR/(n – p)	MSR/MSE
Residuals	p – 1	Sum of square error (SSR) = $\sum(y_i - \hat{y})^2$	Mean square regression (MSE) = SSE/(p – 1)	
Total	n – 1	Total sum of square (TSS) = $\sum(y_i - \bar{y})^2$ = SSR + SSE	-	

จุฬาลงกรณ์มหาวิทยาลัย
Chulalongkorn University

where n = number of run

p = number of parameter

y_i = response from experimental

$\bar{y}$ = average of response from experimental

$\hat{y}$ = response from mathematical model

ii. To define F – value from F distribution table.

F – value from F distribution table = F (α, n – p, n – 1)

where α = confidence level 95%

iii. To compare F – value between ANOVA table and F distribution table

If F – value from ANOVA table has higher than F – value from F distribution table. The mathematical model can be used to predict behavior of experimental.

จุฬาลงกรณ์มหาวิทยาลัย
Chulalongkorn University

APPENDIX K TOTAL ORGANIC COMPOUND

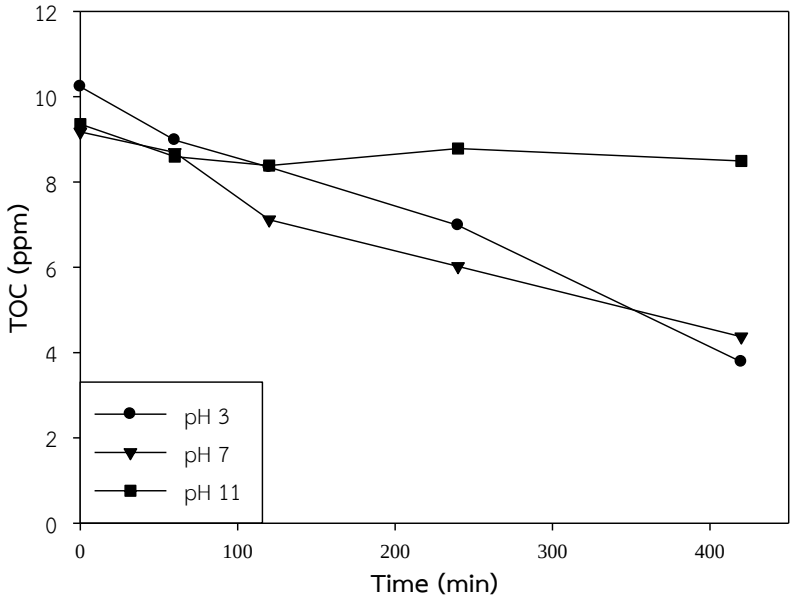

Figure K1 TOC under applied voltage 2.5 V.

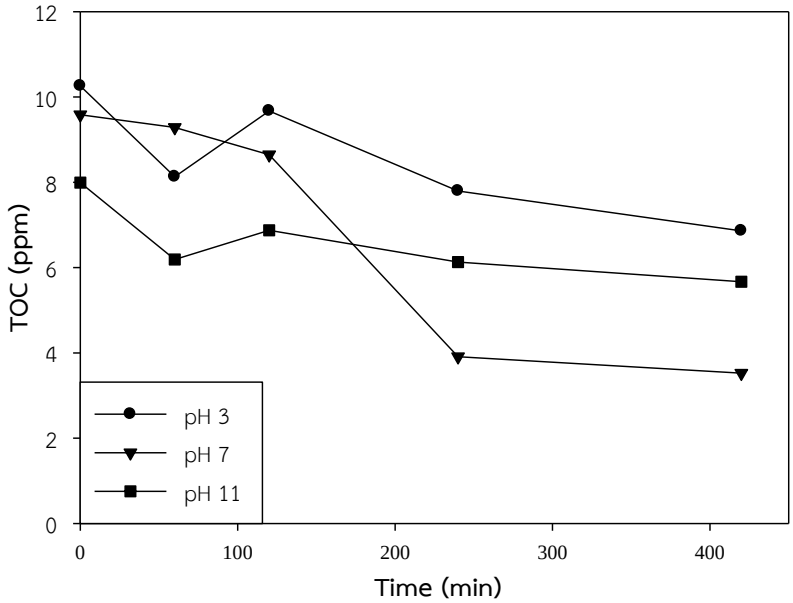

Figure K2 TOC under applied voltage 5 V.

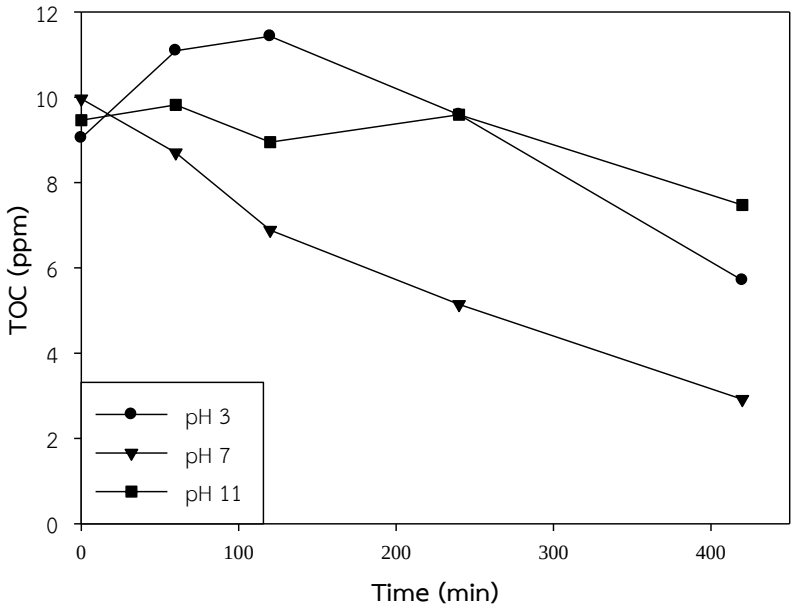

Figure K3 TOC under applied voltage 7.5 V.

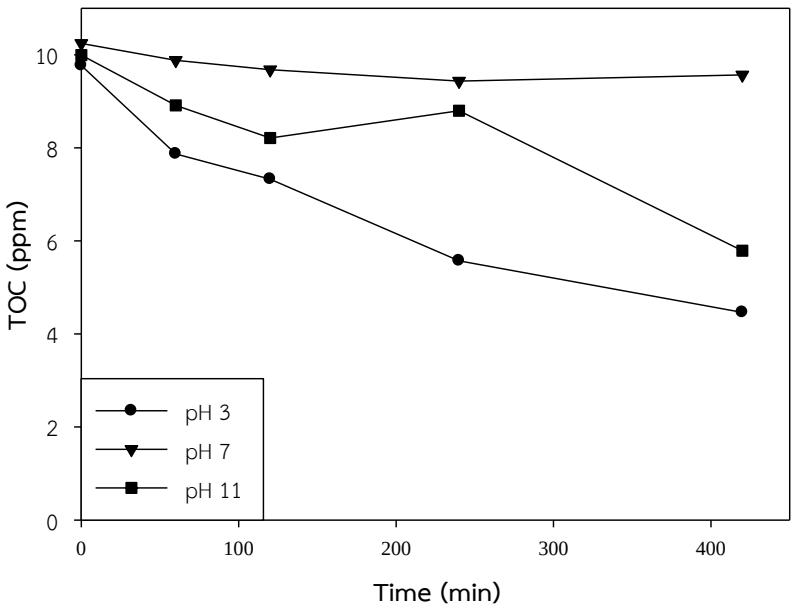

Figure K4 TOC under applied voltage 10 V.

APPENDIX L LIST OF PLUBLICATION

1. Teerapat Raksatham, Chabaiporn Junin, Chanchana Thanachayanont, and Varong Pavarajarn. “PHOTOELECTROCATALYTIC DEGRADATION OF DIURON ON TITANIA FILM”. Pure and Applied Chemistry International Conference 2014 (PACCON2014), Khon Kaen, Thailand, January 8 – 10, 2014.

จุฬาลงกรณ์มหาวิทยาลัย
Chulalongkorn University

VITA

Name:	Mr. Teerapat Raksatham
Date of birth:	May 7th 1989 in Chonburi, Thailand.
Nationality:	Thai
Educational background:	Science and mathematics program, Chonradsadornumrung School, Chonburi, Thailan (2004 – 2006).
	Bachelor's degree of engineering (Chemical engineering), Faculty of engineering, Thammasat university, Bangkok, Thailand (2007 – 2011).
	Master's degree of engineering (Chemical engineering), Faculty of engineering, Chulalongkron university, Bangkok, Thailand.

จุฬาลงกรณ์มหาวิทยาลัย
Chulalongkorn University